เยื่อแผ่นคอมพอสิทของพอลิเมอร์และท่อนาโนคาร์บอนเพื่อใช้จับแก๊สคาร์บอนไดออกไซด์

นางสาวพชรพร ใหญ่สง่า

วิทยานิพนธ์นี้เป็นส่วนหนึ่งของการศึกษาตามหลักสูตรปริญญาวิศวกรรมศาสตรมหาบัณฑิต
สาขาวิชาวิศวกรรมเคมี ภาควิชาวิศวกรรมเคมี
คณะวิศวกรรมศาสตร์ จุฬาลงกรณ์มหาวิทยาลัย
ปีการศึกษา 2560

Carbon nanotube/polymer composite membrane for CO_2 capture

Miss Pacharaporn Yaisanga

A Thesis Submitted in Partial Fulfillment of the Requirements
for the Degree of Master of Engineering Program in Chemical Engineering
Department of Chemical Engineering
Faculty of Engineering
Chulalongkorn University
Academic Year 2017

Thesis Title	Carbon nanotube/polymer composite membrane for CO_2 capture
By	Miss Pacharaporn Yaisanga
Field of Study	Chemical Engineering
Thesis Advisor	Associate Professor Tawatchai Charinpanitkul, D.Eng.
Thesis Co-Advisor	Chalida Klaysom, Ph.D.

Accepted by the Faculty of Engineering, Chulalongkorn University in Partial Fulfillment of the Requirements for the Master's Degree

.....Dean of the Faculty of Engineering
(Associate Professor Supot Teachavorasinskun, D.Eng.)

THESIS COMMITTEE

.....Chairman
(Associate Professor Varong Pavarajarn, Ph.D.)

.....Thesis Advisor
(Associate Professor Tawatchai Charinpanitkul, D.Eng.)

.....Thesis Co-Advisor
(Chalida Klaysom, Ph.D.)

.....Examiner
(Assistant Professor Sorada Kanokpanont, Ph.D.)

.....Examiner
(Assistant Professor Kreangkrai Maneeintr, Ph.D.)

.....External Examiner
(Associate Professor Chirakarn Muangnapoh, Dr.Ing.)

พชรพร ใหญ่สง่า : เยื่อแผ่นคอมพอสิทของพอลิเมอร์และท่อนาโนคาร์บอนเพื่อใช้จับแก๊สคาร์บอนไดออกไซด์ (Carbon nanotube/polymer composite membrane for CO_2 capture) อ.ที่ปรึกษาวิทยานิพนธ์หลัก: รศ. ดร.ธวัชชัย ชรินพาณิชกุล, อ.ที่ปรึกษาวิทยานิพนธ์ร่วม: ดร.ชลิดา คล้ายโสม, 61 หน้า.

การดูดซึมแก๊สคาร์บอนไดออกไซด์ผ่านเยื่อแผ่น เป็นวิธีการที่มีศักยภาพที่โดดเด่น เช่น การปรับอัตราการไหลของแก๊สและของเหลวได้โดยไม่ขึ้นต่อกัน อุปกรณ์มีขนาดกะทัดรัด และการขยายขนาดอุปกรณ์ ปัญหาสำคัญที่เกิดจากการใช้งานในระบบนี้คือการเปียก ซึ่งก่อให้เกิดความเสียหายต่อเยื่อแผ่นและลดประสิทธิภาพในการจับแก๊สคาร์บอนไดออกไซด์ โดยสามารถปรับปรุงคุณสมบัติเยื่อแผ่นให้ทนต่อการเปียกได้โดยเพิ่มคุณสมบัติความไม่ชอบน้ำ ในงานวิจัยนี้เลือกใช้ท่อนาโนคาร์บอนมาปรับปรุงคุณสมบัตินี้ในเยื่อแผ่นพอลิเมอร์พอลิอะคริโลไนไตรล์และพอลิไวนิลิดีนฟลูออไรด์ ผลการศึกษาพบว่าการเติมท่อนาโนคาร์บอนไม่ส่งผลกระทบต่อโครงสร้างและคุณสมบัติความไม่ชอบน้ำของเยื่อแผ่นคอมพอสิทพอลิอะคริโลไนไตรล์ และพบการเปียกหลังการใช้งานไป 30 นาที ทำให้เยื่อแผ่นคอมพอสิทพอลิอะคริโลไนไตรล์ไม่เหมาะสมกับการใช้งานในการดูดซึมแก๊สคาร์บอนไดออกไซด์ผ่านเยื่อแผ่น ในขณะที่การเติมท่อนาโนคาร์บอนส่งผลกระทบต่อโครงสร้างพื้นผิวและคุณสมบัติความไม่ชอบน้ำของเยื่อแผ่นคอมพอสิทพอลิไวนิลิดีนฟลูออไรด์ โดยเยื่อแผ่นคอมพอสิทที่เหมาะสมในการนำมาใช้ในการดูดซึมแก๊สคาร์บอนไดออกไซด์ผ่านเยื่อแผ่นมากที่สุดคือที่ปริมาณการเติมท่อนาโนคาร์บอน 5 % โดยปริมาณในพอลิไวนิลิดีนฟลูออไรด์ ซึ่งมีค่ามุมสัมผัสกับน้ำเท่ากับ 97° รวมถึงมีการกระจายตัวของรูพรุนบนพื้นผิวอย่างสม่ำเสมอด้วยขนาดรูพรุนเฉลี่ยเท่ากับ 254 ± 10 นาโนเมตร และมีประสิทธิภาพในการจับแก๊สคาร์บอนไดออกไซด์เท่ากับ 7.12 mmol/m^2s ซึ่งสูงกว่าเยื่อแผ่นพอลิไวนิลิดีนฟลูออไรด์ถึง 46 % อีกทั้งยังสามารถทนต่อการใช้งานเป็นเวลานานได้โดยไม่มีการเปลี่ยนแปลงทางเคมีที่พื้นผิว และมีการบวมของเยื่อแผ่นเพียงเล็กน้อยเมื่อทำการทดลองเป็นเวลา 30 วัน

ภาควิชา	วิศวกรรมเคมี	ลายมือชื่อนิสิต	.....
สาขาวิชา	วิศวกรรมเคมี	ลายมือชื่อ อ.ที่ปรึกษาหลัก	.....
ปีการศึกษา	2560	ลายมือชื่อ อ.ที่ปรึกษาร่วม	.....

5770240821 : MAJOR CHEMICAL ENGINEERING
KEYWORDS: CARBON DIOXIDE CAPTURE / COMPOSITE MEMBRANE / CARBON NANOTUBES / MEMBRANE GAS ABSORPTION

PACHARAPORN YAISANGA: Carbon nanotube/polymer composite membrane for CO_2 capture. ADVISOR: ASSOC. PROF. TAWATCHAI CHARINPANITKUL, D.Eng., CO-ADVISOR: CHALIDA KLAYSOM, Ph.D., 61 pp.

Membrane gas absorption (MGA) was applied for carbon dioxide capture due to its unique potential, such as independent adjustment of gas and liquid, compact equipment installation, and sizable module. However, a major issue of MGA is membrane wetting, causing lower absorption efficiency and membrane damages. Hydrophobicity is one of the key parameters to improve membrane property for solving such problem. This thesis focused on using carbon nanotubes as the filler to composite with polyacrylonitrile (PAN) or polyvinylidene fluoride (PDVF) via a phase inversion technique to improve membranes hydrophobicity. In case of PAN, the results showed that the addition of CNT exerted insignificant effect on membrane properties and membrane hydrophobicity. Bare PAN and its composite membranes were found to get wetted after the operation for 30 min, suggesting that they would not be suitable for MGA with 3 M monoethanolamine (MEA). In case of PVDF, CNT addition affected surface porosity and also enhanced water contact angle. The best condition of CNT/PVDF composite membrane for CO_2 capture was 5 % by weight of CNT in PVDF matrix, which could exert water contact angle above 97°, uniform pore size distribution, and small pore size (254 ± 10 nm). The CNT/PVDF composite membrane could accommodate absorption flux of 7.12 mmol/m^2s, namely 46 % higher than that of the bare one. Typical long-period operation (> 30 days) showed that the CNT/PVDF composite membrane slightly swelled after contacted with 3 M MEA for 30 days without surface chemical changes, resulted from chemical resistance.

Department:	Chemical Engineering	Student's Signature .....
Field of Study:	Chemical Engineering	Advisor's Signature .....
Academic Year:	2017	Co-Advisor's Signature .....

ACKNOWLEDGEMENTS

Financial support of the Silver Jubilee Fund of Chulalongkorn University through the Center of Excellent in Particle Technology (CEPT) is gratefully acknowledged. This research was funded by the Ratchadapisek Sompoch Endownment Fund (CU-58-064-CC). Thailand Research Fund and Chulalongkorn University via the Institutional Research Grant (IRG 5780014) and Contract No. RES_57_411_21_076 and Grants for Development of New Faculty Staff (Ratchadaphiseksomphot Endownment Fund) are also gratefully acknowledged.

National Nanotechnology Center (NANOTEC) is also appreciated for instrumental supply, and especially thanks to Ms. Chuleeporn Laudthong, NANOTEC - Senior Research Assistant, for her kind suggestion and guidance throughout the experimental setup.

Gratefully thanks to my advisor, Assoc. Prof. Tawatchai Charinpanitkul, and my co-advisor, Dr. Chalida Klaysom, for their kind advice and support. Also, I would like to thank Assoc. Prof. Varong Pavarajarn, as the chairman, Asst. Prof. Sorada Kanokpanont and Asst. Prof. Kreangkrai Maneeintr, as the internal examiners, and Assoc. Prof. Chirakarn Muangnapoh, as the external examiner, for committee participation and useful comments.

Finally, thanks to my friends and my family who always support and give counsel. Indispensably, thanks to all my effort to accomplish this thesis.

CONTENTS

Page

1. Introduction

Carbon dioxide (CO_2) is one of greenhouse gases, which is emitted from various sources, such as industry and transportation. Fossil-fuel power plant is considered the major source of the CO_2 emission as flue gas. There are several techniques employed to capture CO_2 in the post-combustion process, such as absorption, adsorption, and membrane gas separation. The advantages and disadvantages of each post-combustion CO_2 capture techniques are summarized in **Table 1.1**.

Table 1.1 Advantages and disadvantages of each CO_2 capture techniques

Techniques	Advantages	Disadvantages
Absorption	- High efficiency of CO_2 removal - Absorbent regeneration	- Solvent loss by evaporation - Corrosion
Adsorption	- High selectivity (even at a low CO_2 concentration) - Adsorbent recycle	- Need an extreme pre-treatment
Membrane Gas Separation	- High selectivity - Compact device	- Operational problems such as low flux and fouling

Absorption is a conventional approach, which has been used in industry scale due to its high efficiency. Alkanolamines, such as monoethanolamine (MEA) and diethanolamine (DEA), were commonly used as absorbents in industrial CO_2 capture. The liquid absorbent could be also regenerate by heating and/or depressurizing. However, solvent evaporation loss, corrosion, and environmental problems regarding to its toxicity and degradation are still of concern [1].

Adsorption is another promising technique for CO_2 capture because of its high selectivity. Carbon dioxide could be adsorbed on the solid adsorbent surface even at low CO_2 concentration. The commercial adsorbents include activated cabons, zeolites,

alumina, meso-porous silicates, and metal oxide [2]. The adsorbent could be also recycled by swinging the pressure or temperature. Pressure swing adsorption (PSA) is commercially used in the industry instead of temperature swing adsorption (TSA) due to lower energy consumption [3]. However, there is a limitation in cyclic capacity in commercial used [2].

In recent years, membrane gas separation has been developed for the CO_2/N_2 separation from flue gas [1]. The membrane is developed to select a specific gas (CO_2) by the selective thin film, which composite with the non-selective support layer. The advantage of membrane device is its compact size when compared to absorption or adsorption column. However, the efficiency of membrane gas separation is strongly affected by flue gas conditions such as gas contaminants, CO_2 concentration, and pressure. Gas contaminants, such as NO_x and SO_x, cause fouling and membrane damage during the operation [2], while CO_2 concentration and pressure affect CO_2 diffusion and separation efficiency [3]. Membrane for this application is necessarily developed to achieved higher CO_2 flux and purity [2].

There is another alternative process to capture CO_2 that combines the absorption technique with the membrane technique, so called “Membrane Gas Absorption (MGA)”. This technique is different from membrane gas separation technique because the membrane is only used as a barrier to separate gas and liquid phase, so that their flows can be adjusted independently. Thus, CO_2 is not separated by a membrane like in membrane gas separation but by an absorption of solvent [4]. MGA provide higher CO_2 removal rate than membrane gas separation due to higher driving force of CO_2 concentration. The independent control of gas and liquid flow rate results in the lack of entrainment, flooding, and foaming [2]. Porous membranes are often used to minimize membrane resistance and provide higher CO_2 diffusion flux [5]. The membrane device is more compact and easily scaled-up, compared to absorption column [5]. Though, the biggest challenge of the MGA is wetting and the stability of long-term operation. In MGA, membrane is commonly soaked with liquid absorbent that gradually fills the pores of the membrane (wet) and causes membrane swelling and the efficiency decline [6]. To prevent this problem, hydrophobic membrane would be required for the MGA [7, 8]. Membrane is commonly fabricated via phase inversion technique and several approaches have been applied to increase

membrane hydrophobicity such as adjusting membrane morphology [9-11], conducting surface modification [12, 13], and adding hydrophobic additives [14-20].

The additive addition is the simplest and most effective method among all attempts. Carbon nanotubes (CNTs) are one of popular additives, possessing high mechanical strength, light weight, and superhydrophobicity [21]. Previous studies have reported that incorporation of CNTs with polymeric materials could significantly enhance the mechanical strength as well as hydrophobicity of the membranes [22-24]. However, there is still no report of developing CNT composite membranes for using in MGA.

Polyvinylidene fluoride (PVDF) is one of the polymers mostly used in MGA due to its high hydrophobicity and relatively lower cost compared to the higher hydrophobic polytetrafluoroethylene (PTFE). PVDF also showed good potential in MGA system [9, 16, 18, 20]. So, PVDF was selected to use in this research. Polyacrylonitrile (PAN) is another interesting polymer choice. Polyacrylonitrile (PAN) possesses good chemical stability, thermal stability, and mechanical strength which is a good potential for MGA application [25]. Chemical resistance would enhance membrane stability when the membrane expose to the absorbent, and mechanical strength would enhance membrane durability when use under high flow rate condition. Also, thermal stability would enhance membrane stability when use under high temperature condition, such as CO_2 capture from flue gas. However, PAN is quite hydrophilic (water contact angle, 40˚) [26]; due to its high chemical resistance which should be benefit for MGA system. Therefore, if its hydrophobicity could be improved, it could be potentially used in MGA.

1.1 Objectives

The objectives of this study are as follows:

- Synthesis and Characterization of CNT composite polymeric membrane: CNT/PAN and CNT/PVDF
- Investigation of the effects of CNT fillers on membrane morphology and hydrophobicity
- Performance testing of the composite membrane in CO_2 capture in MGA process

1.2 Scope

Membranes were prepared by a phase inversion with controlled parameters listed below.

- Polymer matrix: Polyacrylonitrile (PAN) and Polyvinylidene fluoride (PVDF)
- Solvent: *N*,*N*-dimethylformamide (DMF)
- Polymer concentration: 12 – 28 % by weight
- CNT loading: 0 – 10 % by weight in polymer

1.3 Expected Outcomes

CNT adding would improve hydrophobicity of membrane surface and enhance CO_2 capture efficiency in MGA system.

2. Background and Literature Review

The background knowledge of membrane gas absorption (MGA) and membrane preparation via phase inversion technique were discussed below. Recent developed membranes for the MGA were also discussed in detail in this chapter.

2.1 Membrane Gas Absorption (MGA)

Membrane employed for gas absorption is often called membrane contactor, which allows gas phase to contact liquid phase without dispersing one to another. Therefore, gas and liquid flow rate can be adjusted and manipulated independently without flooding, foaming, and channeling, which are normally an obstacle in an absorption column. Moreover, membrane device is more compact when compares to the same operational volume of column, leading to less installation area and energy consumption [5]. Different from conventionally absorption column, the mass transfer in MGA occurs in 3 steps;

1) Gas diffusion from bulk to membrane surface

2) Gas diffusion through the membrane pores

3) Dissolution of gas into liquid phase

Membrane provides the main mass transfer resistance in this system. In MGA system, CO_2 and other gases could diffuse through the membrane from gas-side to liquid-side, but CO_2 will be absorbed by the absorbent. In case of CO_2, CO_2 could diffuse through membrane porosity by Knudsen diffusion if the scale of pore diameter is higher than CO_2 mean free path (39 nm at 0 ˚C and atmospheric pressure) and Fick's law of diffusion due to the different of CO_2 concentration. In the case of membranes with finger-liked pore structure, CO_2 could easily diffuse through membrane straight pore. While in case of sponge-like pore structure, the membrane pores were more tortuous. The porosity (ε) and tortuosity (τ) are the parameters determining the mass transfer coefficient (k_m) [27]. In the case of thin film layer, CO_2 may diffuse through the dense thin film by solution-diffusion, resulted from concentration gradient [27]. However, the gas could diffuse through the chain of polymer in random direction. Therefore, to minimize membrane resistance, the

membrane thickness should be minimized. In addition, membrane used in the MGA are highly porous.

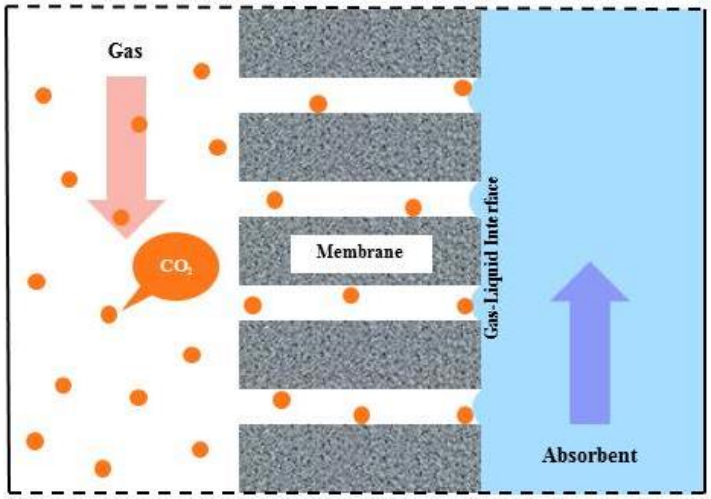

Fig 2.1 Membrane gas absorption principle

The instance of CO_2 capture by a MGA is shown in **Fig 2.1**. In a flat-sheet membrane system with gas physical absorption, the over-all mass transfer coefficient is calculated by the following equation [10]:

$$K_i(m/s) = \frac{Q_g(C_{i,g,in} - C_{i,g,out})}{A_m(\Delta C_m)} \quad (1.1)$$

where K_i is over-all mass transfer coefficient, Q_g is the volumetric flow rate of gas phase, A_m is the area of the membrane and ΔC_m is the logarithmic mean driving force based on gas phase concentration [10]:

$$\Delta C_m = \frac{(HC_{i,g,in} - C_{l,out}) - HC_{i,g,out}}{\ln[(HC_{i,g,in} - C_{l,out})/(HC_{i,g,out})]} \quad (1.2)$$

where $C_{i,g,in}$ and $C_{i,g,out}$ are the concentration of the gas inlet and outlet, respectively. While $C_{l,out}$ is the CO_2 concentration in the liquid outlet. And H is the Henry's constant of the interested gas in the liquid absorbent.

The CO_2 diffusional flux can be expressed by the following equation [9, 10]:

$$J_{CO_2} = K_i(c_g - c_l^*) \quad (1.3)$$

where J_{CO_2} is the CO_2 absorption flux (mol/m^{2}s); c_g is the concentration in gas phase (mol/m^3) and c_l^* is the gas phase concentration in equilibrium with the bulk

liquid phase (mol/m^3). Also, the CO_2 removal efficiency (η) can calculate by using the following equation [9]:

$$\eta = \frac{C_{i,g,in} - C_{i,g,out}}{C_{i,g,in}} \times 100 \quad (1.4)$$

Important operation parameters that influence CO_2 absorption are gas and liquid flow rates, which could directly affect over-all mass transfer coefficient. The higher the gas flow rate, the less the resistance of stagnant layer diffusion [28]. However, excessively high gas flow rate leads to excessively short residence time in the membrane module, resulting in lower CO_2 removal [29]. Also, the higher liquid flow rate leads to thinner liquid boundary thickness, resulting in higher over-all mass transfer coefficient and CO_2 absorption flux [30]. Therefore, for each module, the gas and liquid velocity should be adjusted to maintain enough residence time and CO_2 absorption flux for CO_2 removal.

A hydrophobic membrane is normally required to keep the liquid flow along membrane surface instead of filling in the pores, causing wetting. When the membrane pore was filled and fully wet, its effective area reduces. The liquid solvent could capture CO_2 only in pore area and thus the mass transfer resistance of the wetted membrane increases, leading to less CO_2 absorption flux [5]. Moreover, membrane would be damaged by membrane-absorbent interaction, leading to a less mechanical strength [31, 32].

In general, commercial liquid absorbent for CO_2 capture is an organic compound, which possesses low surface tension [6]. Monoethanolamine (MEA) is considered as one of the promising absorbents for the CO_2 capture. Higher MEA concentration is required to highly remove CO_2 but it generates less surface tension that make the MEA easily penetrate into membrane pores. Thus, the selection of hydrophobic membrane and the adjustment of operational parameters should be carefully applied to keep the liquid flow along membrane surface instead of filling in the pores, causing wetting [5].

2.2 Membrane Preparation

Phase inversion, in which a polymer is transformed from a liquid to a solid state in a controlled manner, is the most commonly technique in membrane production in both commercial and laboratory scale [33]. Variety of characteristic membrane structures is gained from this technique by adjusting phase inversion parameters [34]. In general, polymers are dissolved in a solvent to form a homogeneous polymer solution and cast on a plate or a non-woven support. Afterwards, the cast polymer solution is left in the air or immersed in a non-solvent coagulation bath (or both means) where polymer precipitation occurs to form a membrane flat sheet by solvent evaporation or solvent/non-solvent exchange, respectively [35]. In polymer/solvent/non-solvent ternary phase system, polymer-rich and -lean phase occurs when the temperature of polymer solution was lowered [35]. Polymer-rich phase leads membrane structure formation, whereas polymer-lean phase leads membrane void formation by liquid-liquid demixing process [36]. Demixing process was divided into 2 paths: instantaneous demixing and delayed demixing, leading to different membrane structures. Exchange rate of solvent and non-solvent is the key to determine what kind of demixing process occurs. When the cast polymer solution is immersed in a non-solvent coagulation bath, polymer nearby the polymer solution and non-solvent interface firstly precipitates, leading to thin skin-layer formation, which becomes a non-solvent in-flow barrier, while the amount of non-solvent in-flow before skin-layer formation induces the diffusion of solvent at the sub-layer [35]. For the sub-layer, solvent diffusion will also occur between polymer-rich and –lean phase, called solvent imbibition [37]. If the solvent imbibition grows fast, fast polymer precipitation will occur. This is referred to the instantaneous demixing, in which the macrovoids and finger-like pore tend to form in membrane structure [38]. Whereas in a delayed demixing, sponge-liked pore structure is formed because polymer-lean phase seeds could not grow and polymer-rich phase slowly precipitate [39]. Many preparation parameters such as solvent/non-solvent choice, type of polymer, and polymer concentration have influences on membrane morphology. Solvent/non-solvent pairs have direct impact on demixing time because their miscibility takes action for exchange rate [26, 38]. The selection of polymer depends on the required properties of the membrane such as hydrophobicity and thermal and

chemical resistance [26]. Moreover, adding additives as a third component of casting solution may affect the demixing path way and the membrane structure [26].

2.3 Literature Review on Membrane Developments for MGA

Membrane mostly used in MGA for CO_2 capture is made of hydrophobic polymers, such as polytetrafluoroethylene (PTFE) (water contact angle, 109.4˚), polyvinylidene fluoride (PVDF) (water contact angel, 86.0˚), polyetherimide (PEI) (water contact angle, 76.5˚), and polysulfone (PSF) (water contact angle, 75.0˚).

While hydrophobicity plays a role in maintaining membrane long-term operation, pore size and porosity mainly determines the CO_2 removal performances. A good MGA membrane requires small pore size but high porosity to enhance CO_2 diffusion and decrease the opportunity of absorbent wetting [10]. All properties and performance data obtained from previous reports were summarized in **Table 2.1**.

Table 2.1 Properties and performance of membranes recently developed for MGA system

Polymer Concentration (wt%)	Additives	Water Contact Angle (˚)	Porosity (%)	Avg. Pore Size (nm)	Testing Conditions	CO_2 Absorption Flux (mol/m^{2}s)	Ref.
Polyvinylidene fluoride (PVDF)							
15-20	-	127.2	90	35[a]	20%CO_2/N_2-AMP Q_l = 1500 ml/min Q_g = 3600 ml/min	N/A	[9]
20	-	90	55	310	20%CO_2/N_2-AMP Q_l = 2500 ml/min Q_g = 3600 ml/min	420	[10]
18	1 wt% SMM	92	N/A	385	CO_2-Water Q_l = 300 ml/min Q_g = 100 ml/min	7.7×10^{-4}	[17]
17	2 wt% SMM	96.2	N/A	200	CO_2-Water Q_l = 80 ml/min Q_g = 100 ml/min	4.5×10^{-4}	[14]
18	6 wt% SMM	99	85	654	CO_2-Water Q_l = 300 ml/min Q_g = 100 ml/min	5.4×10^{-3}	[16]
18	1 wt%[b]	90	N/A	28.7	CO_2-Water	1×10^{-3}	[18]

Polymer Concentration (wt%)	Additives	Water Contact Angle (˚)	Porosity (%)	Avg. Pore Size (nm)	Testing Conditions	CO_2 Absorption Flux (mol/m^2s)	Ref.
	MMT				V_l = 3.1 m/s Q_g = 140 ml/min		
18	5 wt%[b] MMT	99	N/A	21	CO_2-Water Q_l = 200 ml/min Q_g = 1400 ml/min	1.65×10^{-3}	[20]
Polyetherimide (PEI)							
16	(Modified with 2% Octadecylamine solution)	111.5	N/A	N/A	CO_2-Water V_l = 0.1 m/s	2.2×10^{-3}	[11]
14	(Dope with Fluorinated Silica)	124	81	40	CO_2-Water V_l = 0.3 m/s Q_g = 30 ml/min	1.6×10^{-3}	[12]
14	(Dope with Fluorinated Silica)	123.2	71.2	90	CO_2-Water V_g = 0.12 m/s	3×10^{-3}	[13]
					CO_2-Sodium Tuarinate V_g = 0.8 m/s	2.1×10^{-2}	
15	1 wt%[b] MMT	86	N/A	79	CO_2-Water V_l = 0.5 m/s	1.09×10^{-3}	[19]
Polysulfone (PSF)							
15	1 wt% SMM	73	83	568	CO_2-Water Q_l = 300 ml/min Q_g = 100 ml/min	5.8×10^{-4}	[15]
Polypropylene (PP)							
N/A	-	158	N/A	200	20%CO_2/N_2-MEA Q_l = 17 ml/min Q_g = 200 ml/min	1.9×10^{-4}	[31]

[a] maximum pore size

[b] % by weight in polymer

Hydrophobic property highly depends on membrane surface properties such as pore size, porosity, roughness, and chemical properties [6]**.** So, there are many attempts to improve membrane hydrophobicity for more effective usage. There are 3 main approaches to improve membrane hydrophobicity: adjusting membrane

morphology, modifying membrane surface, and adding an inducing hydrophobic additives [5].

Via /the first approach, non-solvent additives were added in polymer solution during phase inversion step to adjust membrane morphology in the way that promotes high contact angle. Non-solvent additives, such as ethanol and *N*-Methyl-2-Pyrrolidone (NMP), were added into water coagulation bath for PVDF precipitation step, resulting in membrane with smaller pore size and an increased water contact angle of 88.8 - 127.2˚ [9, 10].

The second approach is modifying surface of membranes by doping fluorinated silica on PEI [12, 13] or plasma treatment on PVDF [28], which resulted in water contact angle of 124˚ and 155˚, respectively. Surface roughness and fluoro-compounds were modified on the membrane surface to improve membrane hydrophobicity.

In the last approach, hydrophobic additives were directly mixed in polymer solution to improve the hydrophobicity of the polymer matrix. 1 - 6 % by weight of surface modifying macromolecules (SMM) were mixed in the polymer solution to form a membrane through a wet spinning process, which resulted in water contact angle of 92 - 99˚ for PVDF [14, 16, 17] and 70 - 73˚ for PSF [15]. SMM additive provided fluoro-compounds on the membrane surface which improved membrane hydrophobicity, even though membrane pore size and porosity was relatively higher than those of the bare one. Another hydrophobic additive is montmorillonite (MMT), which was used in a range of 1 - 5 % by weight in PVDF and resulted in water contact angle of 90 - 99˚ for PVDF [18, 20] and 86˚ for PEI [19]. MMT addition caused smaller membrane pore size and more surface roughness than those of the bare one, leading to more membrane hydrophobicity. All 3 approaches mainly affected membrane surface morphology, leading to the change in water contact angle and hydrophobicity.

Membrane porosity and pore size also affect CO_2 absorption flux. High surface porosity leads to preferable CO_2 removal efficiency [9, 16, 18], while small membrane surface pore could prevent membrane wetting [18]. Thus, proper membrane structure for MGA system should be high surface porosity with small pore size [18].

This thesis focused on a synthesis and characterization of a composite membrane to be used in membrane gas absorption for CO_2 capture. The membrane was synthesized by a phase inversion method. PAN and PVDF were used as the polymer matrix and CNT as the filler. Their morphology, surface properties, and CO_2 absorption performance were also investigated.

3. Methodology

3.1 Materials

Polyacrylonitrile (PAN, average M_w = 150,000) and polyvinylidene fluoride (PVDF, average M_w = 275,000) were purchased from Sigma–Aldrich®. *N,N*-dimethylformamide (DMF, AR Grade) and carbon nanotubes (CNTs, baytubes® C 150 P) were supplied by QRëC® and Bayer Material Science, respectively. Monoethanolamine (MEA, 99.5 %) was purchased from Dow Chemical Company (Dow®). All chemicals were used as-received without further purification.

3.2 Fabrication of bare and composite membranes

Polymer was dissolved in solvent, DMF, in a range of 12 to 28 % by weight under a stirring condition at 60 ˚C until the homogeneous solution was obtained. Afterwards, the polymer solution was cooled down to the room temperature and was cast on a non-woven support (novatexx 2470, viledon®) with a constant thickness of 250 μm. The nascent cast film was immediately immersed in water to form a membrane flat sheet.

CNT content was varied in a range of 0 - 10 % by weight in polymer to fabricate composite membranes. The CNT was first dispersed in DMF by using sonication bath for 30 min. Then, polymer was dissolved in the suspended solution at 60 ˚C under a stirring condition until the solution became homogeneous. Afterwards, sonication was further applied for 90 s to ensure a good dispersion of CNT. The mixed solution was then cast on a non-woven support with the same thickness and then immersed in the water bath to form a composite membrane. Carbon black (CB, conductive carbon black, ENSACO®) was also used to composite with polymeric membrane (at 5 % by weight) for a comparison whether different carbon material affects membrane hydrophophobicity. All the conditions synthesized in this thesis were summarized in **Table 3.1**.

Table 3.1 Summary of all experimental compositions used in this thesis

Name	Polymer Concentration (% by weight)	CNT Content (% by weight in polymer)
PAN Membranes		
12 wt% PAN	12	-
14 wt% PAN	14	-
16 wt% PAN	16	-
18 wt% PAN	18	-
Composite PAN Membranes		
0.5 wt% CNT/PAN	12	0.5
1 wt% CNT/PAN	12	1
5 wt% CNT/PAN	12	5
10 wt% CNT/PAN	12	10
5 wt% CB/PAN	12	5*
PVDF Membranes		
22 wt% PVDF	22	-
24 wt% PVDF	24	-
26 wt% PVDF	26	-
28 wt% PVDF	28	-
Composite PVDF Membranes		
0.5 wt% CNT/PVDF	26	0.5
1 wt% CNT/PVDF	26	1
5 wt% CNT/PVDF	26	5
10 wt% CNT/PVDF	26	10
5 wt% CB/PVDF	26	5*

*Carbon Black (CB) was used instead of CNT

3.3 Characterization

3.3.1 Structure and Morphology

Microscopic structure and morphology of the synthesized membranes were investigated by using a scanning electron microscopy (SEM, S-3400N, Hitachi) at their top surfaces and cross-sectional areas. Moreover, particle shape and size of CNTs and CB, as an additive, were also investigated by using a field emission scanning electron microscopy (FE-SEM, JSM-7610F, JEOL) and a transmission electron microscopy (TEM, JEM-2100, JEOL).

3.3.2 Pore Size, Pore Size Distribution, Surface Porosity, and Thickness

Average pore size, pore size distribution and surface porosity of the fabricated membranes were also estimated from SEM micrographs by an image processing program (ImageJ 1.50i, National Institutes of Health, USA) to investigate the effect of polymer concentration and CNT content on membrane morphology. Thin top layer thickness of the fabricated membranes was also measured by using an image processing program (SemAfore 5.21, JEOL, Sweden**).** Also, the whole membrane thickness was measured by using a digital caliper (101-2601, TLEAD).

3.3.3 Porosity

Liquid replacement method was used to investigate membrane porosity. Flat synthesized membranes were cut into the dimension of 3 × 1 cm and weighed as the mass of dry membrane. Then the membranes were storing in 1-octanol (99%, PanReac AppliChem) and deionized water for 2 h and wet membrane weight was recorded. Membrane porosity was calculated by using the following equation [9]:

$$\varepsilon = \frac{m_n/\rho_n}{m_n/\rho_n + m_p/\rho_p} \times 100\% \qquad (3.1)$$

where ε is the porosity of the membrane, m_n is the mass of the absorbed liquid (wet membrane weight – dry membrane weight), m_p is the mass of the dry membrane, ρ_n is the density of liquid, and ρ_p is the density of polymer. (Noted that there was an error from a non-woven support weight and density change of composite membrane.)

Different liquids were used to investigate their absorption ability. The organic liquid representing low surface tension liquid was 1-octanol, which possesses surface tension of 27.60 mN/m at 20 ˚C. The liquid representing high surface tension was water, which possesses surface tension of 72.80 mN/m at 20 ˚C.

3.3.4 Hydrophobicity

To determine hydrophobicity, water contact angle of the fabricated membranes was measured by using contact angle meter (OCA 40, Data Physics).

3.3.5 Surface Roughness

Surface roughness of the fabricated membranes was measured by atomic force microscopy (AFM, NanoScope® IV). The surface roughness could represent how polymer precipitated and often relates to surface hydrophobicity.

3.3.6 Surface Chemicals

Surface chemicals of membranes were examined by using attenuated total reflectance Fourier transform infrared spectroscopy (ATR-FTIR, Nicolet™ 6700, Thermo Scientific). Surface chemical changes of membranes before and after being contacted with the solvent (3 M MEA) up to 30 days were also investigated.

3.3.7 Thermal Resistance

Thermal resistance of the fabricated membranes was further estimated to investigate the effect of carbonaceous additives on membrane thermal stability. The thermal resistance of the fabricated membranes was analyzed by using a thermogravimetric analysis (TGA, TGA/DSC1 STAR^e System, METTLER TOLEDO).

3.4 Performance Test

Performance of the membranes in MGA system was tested in the assemble module shown in **Fig. 3.1** with 3 M MEA as an absorbent. The experiment was conducted at ambient temperature and pressure. The gas and liquid flow rate were

adjusted to avoid gas bubble in the liquid channel. Pure CO_2 (99.995 %, Praxair) was fed into the gas-side of the module through a mass flow meter (SLA5800 Series, BROOKS®) at 320 ml/min and 3 M MEA was circulated into the liquid-side of the module through a peristaltic pump at 157 ± 6 ml/min. Due to the limitation of membrane contacted area and CO_2 detection, the CO_2 captured MEA was collected after 30 min of the operation and then the CO_2 captured amount was measured by a titration method. CO_2 absorption flux was calculated by the following equation:

$$J_{CO_2} = \frac{n_{Absorbed\ CO_2}}{t \times A_m} \tag{4.1}$$

where J_{CO_2} is CO_2 absorption flux (mol/m^{2}s), $n_{Absorbed\ CO_2}$ was the amount of absorbed CO_2 measured and calculated from titration method, t was the operation time (1800 s), and A_m was the contacted area of membrane in the module (0.0024 m^2).

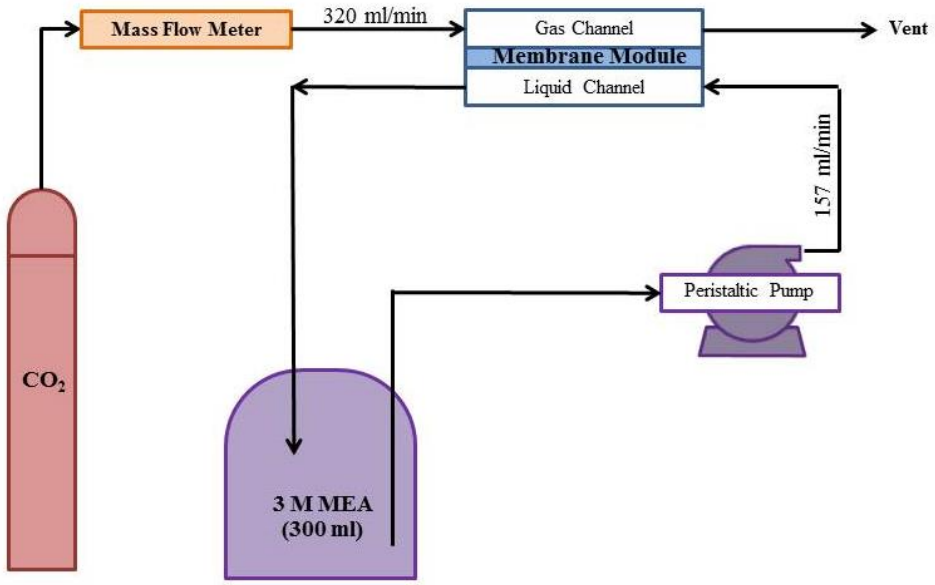

Fig 3.1 Performance test diagram

4. Results and Discussion

In MGA system, membrane is used as a barrier, which adds the resistance to gaseous and liquid mass transfer. To minimize the membrane resistance, membrane with thinner layer, more porous structure, and more surface porosity are required. Moreover, smaller pore size is also required to reduce membrane wetting when the membrane is exposed to liquid absorbent in long-term operation.

In this thesis, two types of membranes, namely PAN and PVDF, were fabricated to investigate their feasibility in MGA application. The results of those membranes were explained and divided into 4 sections as follows.

4.1 PAN Membranes

4.1.1 PAN Membrane Morphology Screening

PAN concentration was varied from 12 to 18 % by weight to fabricate polymeric membranes. Structure of the fabricated membranes consisted of thin top layer and finger-liked pore. The thin top layers of all fabricated membranes were dense with no measurable pores as shown in **Fig. 4.1**. Macrovoids (finger-liked pore structure) were grown by imbibition of solvent diffusing from polymer-rich phase to polymer-lean phase. Then the polymer-rich phase could precipitate as the wall of macrovoids [35]. The whole membrane thickness of PAN membrane with 12, 14, 16, and 18 % by weight was 275 ± 5, 227 ± 8, 217 ± 9, and 197 ± 8 μm, respectively. While the thin top layer thickness was 1.00 ± 0.20, 2.92 ± 0.56, 3.18 ± 0.52, and 3.35 ± 0.34 μm, respectively. The whole membrane thickness decreased with an increase in PAN concentration but the thin top layer was thicker with an increase in PAN concentration. As a result from PAN membrane morphology, the thin top layer showed the main mass transfer resistance when using in MGA system due to its dense skin. Membrane porosity could be determined by the amount of displacement liquid (1-octanol or deionized water) in the pore. The result showed a narrow range of porosity at 52 - 60 % for 1-octanol and 41 - 54 % for deionized water for all membranes (see **Fig. 4.2**).

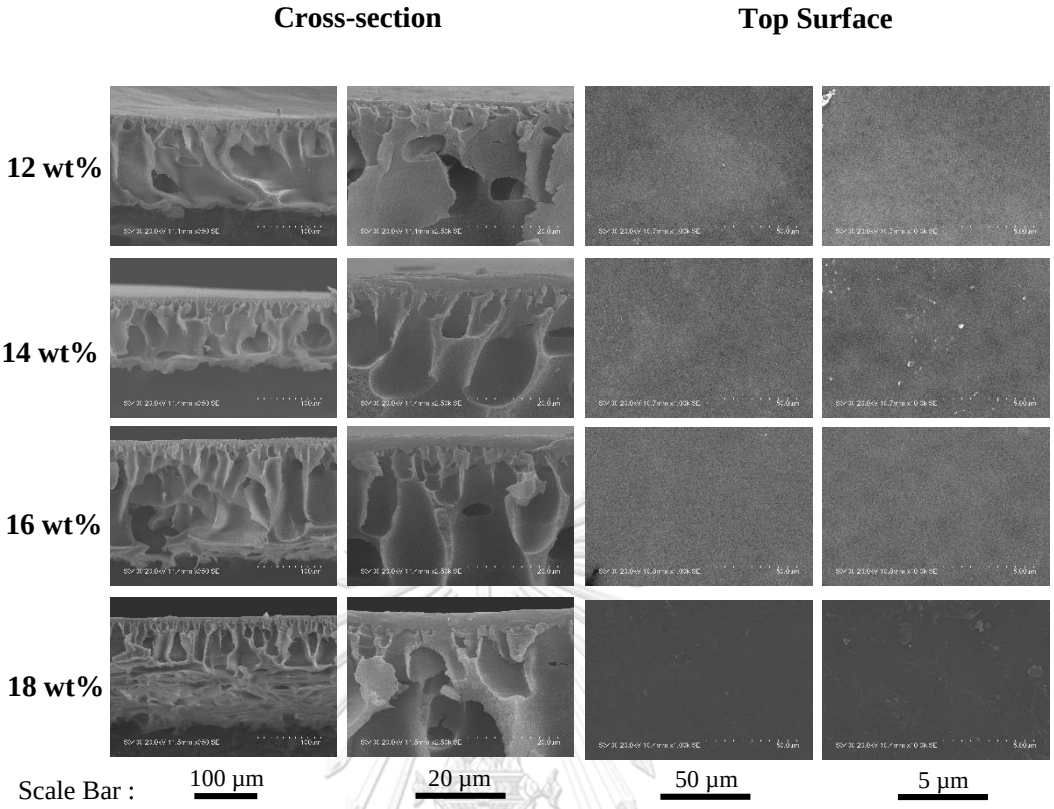

Fig. 4.1 SEM images of PAN membranes

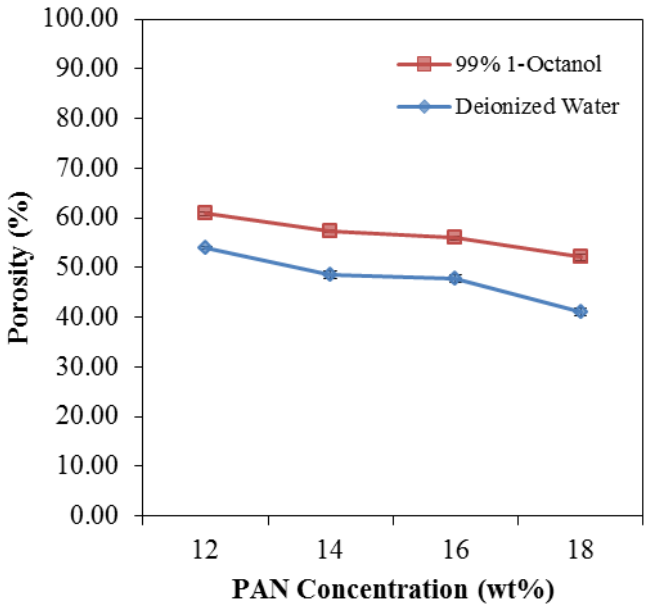

Fig. 4.2 Porosity of PAN membranes

Fig. 4.2 also showed that 1-octanol could more easily penetrate into membrane pore than water due to its lower surface tension (27.60 and 72.80 mN/m, for 1-octanol and water, respectively). However, the difference in liquid surface tension could not make a much difference in membrane liquid absorption. The porosity of PAN membranes from water absorption was closely high to that from 1-octanol absorption, which showed that PAN membranes were hydrophilic [6].

Water contact angle measurement results also confirmed that all PAN membranes were hydrophilic with contact angle below 90˚ as shown in **Fig. 4.3**.

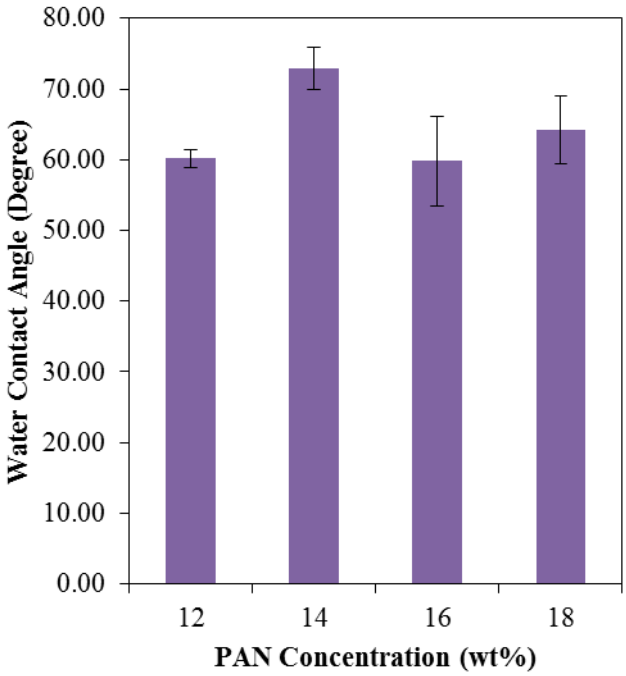

Fig. 4.3 Water contact angle of PAN membranes

All of these results showed that typical PAN membranes fabricated from different polymer concentration exhibited indifferent properties. To minimize membrane resistance in MGA, 12 wt% PAN membrane was selected to composite with CNTs because it possessed the thinnest top thin layer.

4.1.2 CNT/PAN Composite Membranes

PAN membrane with 12 % by weight was composite with varied carbon nanotube content from 0.5 – 10 % by weight in PAN. Morphology of CNT/PAN composite membrane was found to be the same as bare PAN membrane as shown in **Fig. 4.4**.

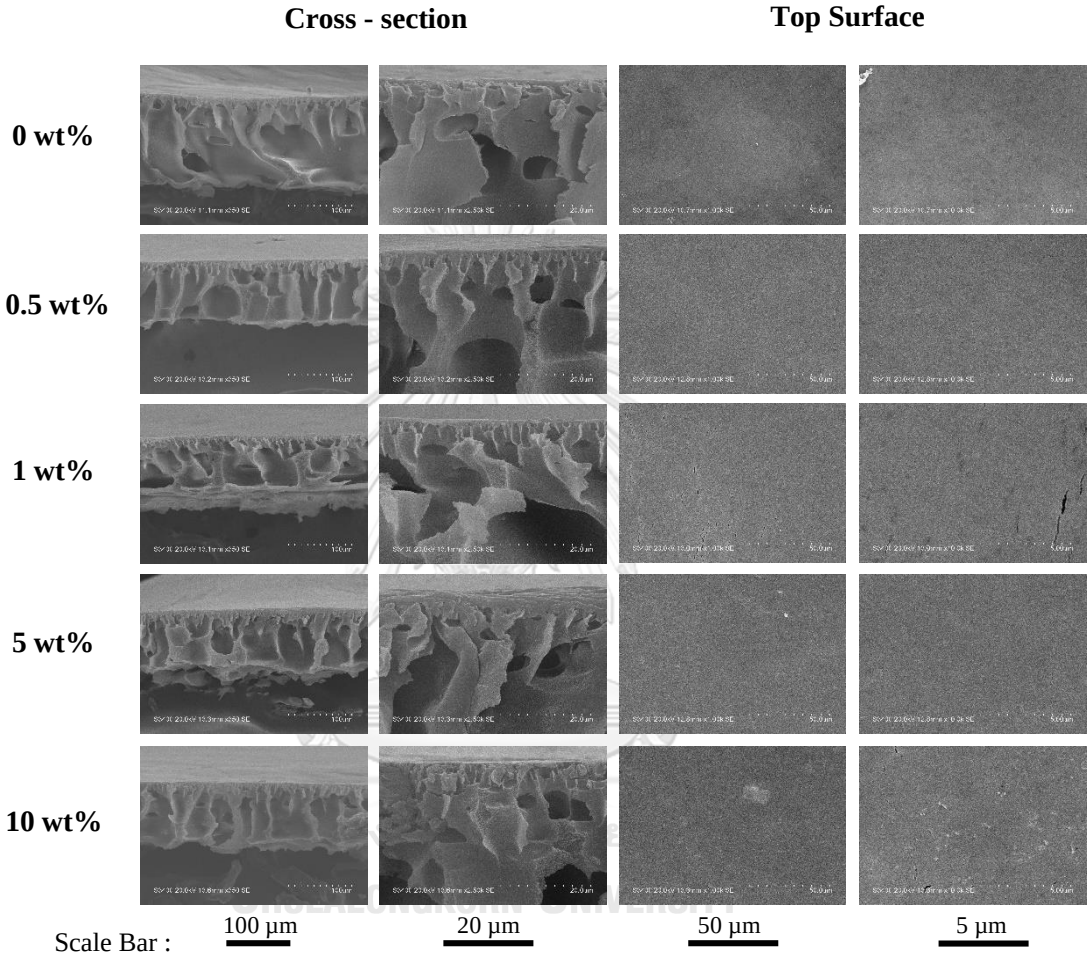

Fig. 4.4 SEM images of CNT/PAN composite membranes

CNT/PAN composite membranes consisted of thin top layer and finger-liked pore structure similar to the bare PAN membranes. Also, the top surfaces of all membranes were dense. These results showed that the addition of CNT (0.5 - 10 % by weight in polymer) has no significant effects on membrane morphology. Furthermore, the whole membrane thickness of CNT/PAN composite membranes was in the range of 194 – 275 µm, and the thin top layer of all CNT/PAN composite membrane was lower than that of the bare one (< 1 µm).

Porosity of CNT/PAN composite membranes was measured and plotted in **Fig 4.5**. Narrow range of porosity measured from two different solvents, 54 - 61 % for 1-octanol and 51 - 54 % for deionized water, was observed. This implied that the CNT/PAN composite membrane was still hydrophilic.

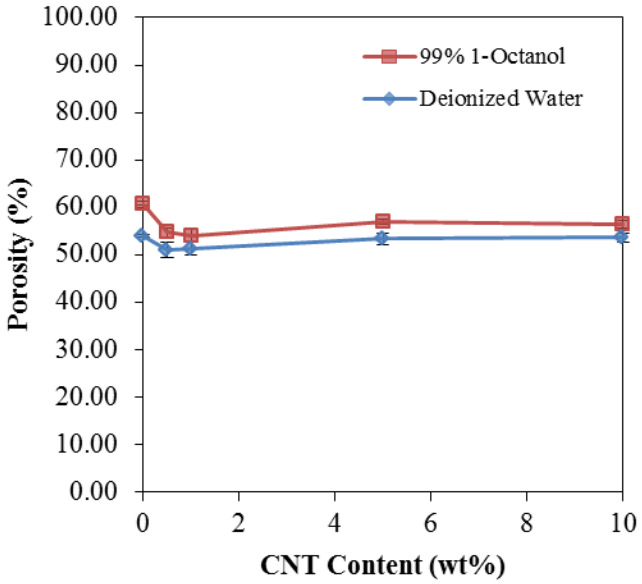

Fig. 4.5 Porosity of CNT/PAN composite membranes

Water contact angle of all CNT/PAN composite membranes was showed in **Fig. 4.6**. All CNT/PAN composite membranes exhibited hydrophilicity with water contact angle below 90˚. The addition of small amount of CNT only slightly improved membrane hydrophobicity. The dense and smooth surface of the composite membranes was the key parameter for regulating water contact angle and hydrophilicity [25].

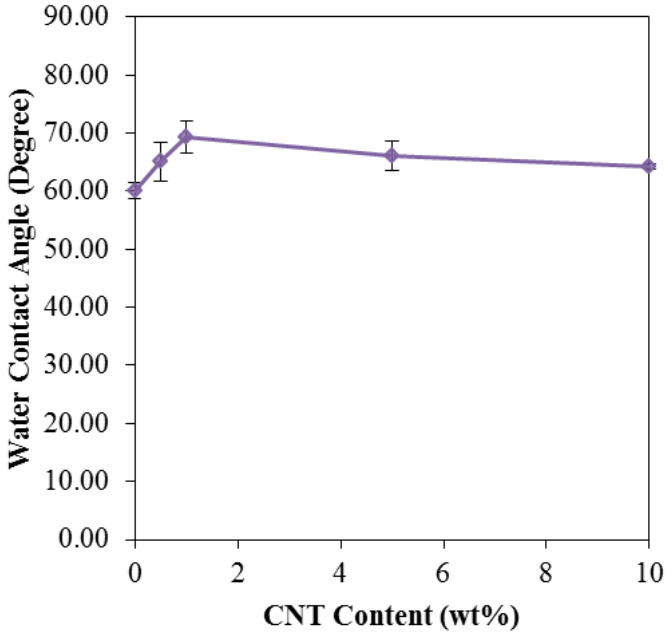

Fig. 4.6 Water contact angle of CNT/PAN composite membranes

4.2 PVDF Membranes

4.2.1 PVDF Membrane Morphology Screening

PVDF concentration was varied from 22 to 28 % by weight to prepare polymeric membrane. The synthesized membranes consisted of 3-layer structure; thin top layer, finger-liked middle layer, and sponge-liked bottom layer. The top surfaces of PVDF membrane were porous as shown in **Fig. 4.7**. The whole thickness of PVDF membranes was in a range of 142 – 154 μm.

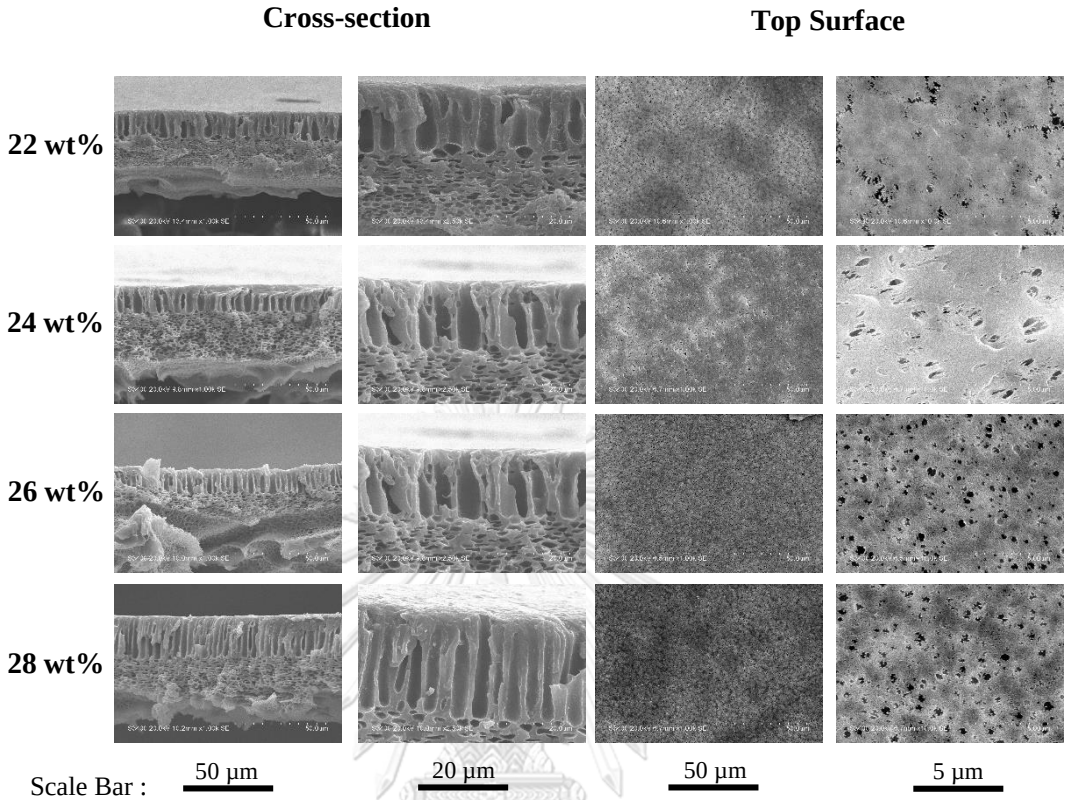

Fig. 4.7 SEM images of PVDF membranes

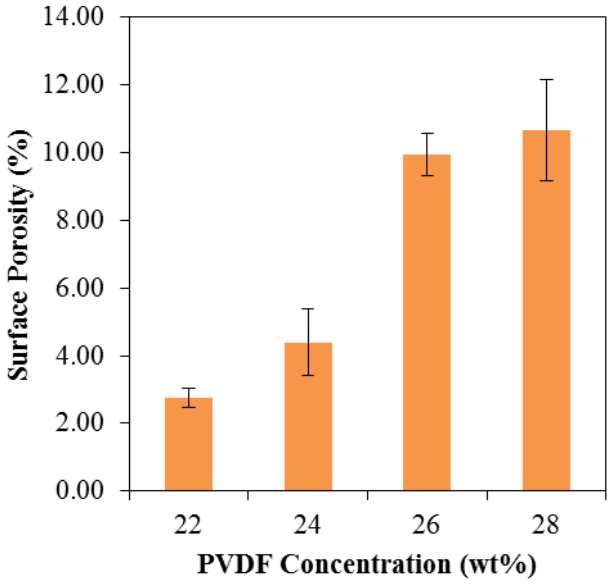

Fig. 4.8 Surface porosity of PVDF membranes

Typical SEM images showed that the top surface of PVDF membrane became more porous with an increase in PVDF concentration. Dependence of PVDF membrane surface porosity on PVDF concentration was plotted in **Fig. 4.8**. Representative size of the surface pores was normally determined by seed size of the polymer-lean phase, which was dispersed in the polymer solution. The seeds would be different by the solution system, especially the difference of polymer concentration [39]. The finger-liked middle layer was formed by the influence of non-solvent inflow from the surface pores, resulting in the growth of macrovoids [37, 40]. The sponge-liked bottom layer was formed by solvent imbibition taking place between the polymer-rich and -lean phase. The seeds of polymer-lean phase were dispersed over the solution bottom layer and the seeds could not grow as macrovoids, leading the sponge-liked forming at the bottom layer [39].

Surface porosity was estimated by using an image processing technique and showed in **Fig. 4.8**. The pore size distribution of surface pores was also estimated and plotted in **Fig. 4.9**. Pore size distribution plots showed that surface pore size of PVDF membrane from the SEM images in **Fig. 4.7**, 26 and 28 wt% PVDF membranes showed pore dispersion with normal distribution and standard deviation of 8 and 11 nm, respectively, which was more uniform than others.

As shown in **Fig. 4.10**, porosity of PVDF membranes exposed to 1-octanol was varied in a range of 46 – 54 %, whereas exposing PVDF membranes to deionized water could provide PVDF membrane with very low porosity in a range of 0 – 2 %. The much lower porosity of PVDF membranes when it was exposed to deionized water might be due to the hydrophobicity of the PVDF that could expel water in the controlled experimental time.

Water contact angle was measured as shown in **Fig. 4.11**. The water contact angle increased with an increase in polymer concentration. It is well-known that contact angle depends on surface properties and chemical properties of material. In this case, the enhance of surface porosity when PVDF concentration increased from 24 % by weight of PVDF (4.39 %) to 26 % by weight of PVDF (9.94 %) seemed to promote the water contact angle.

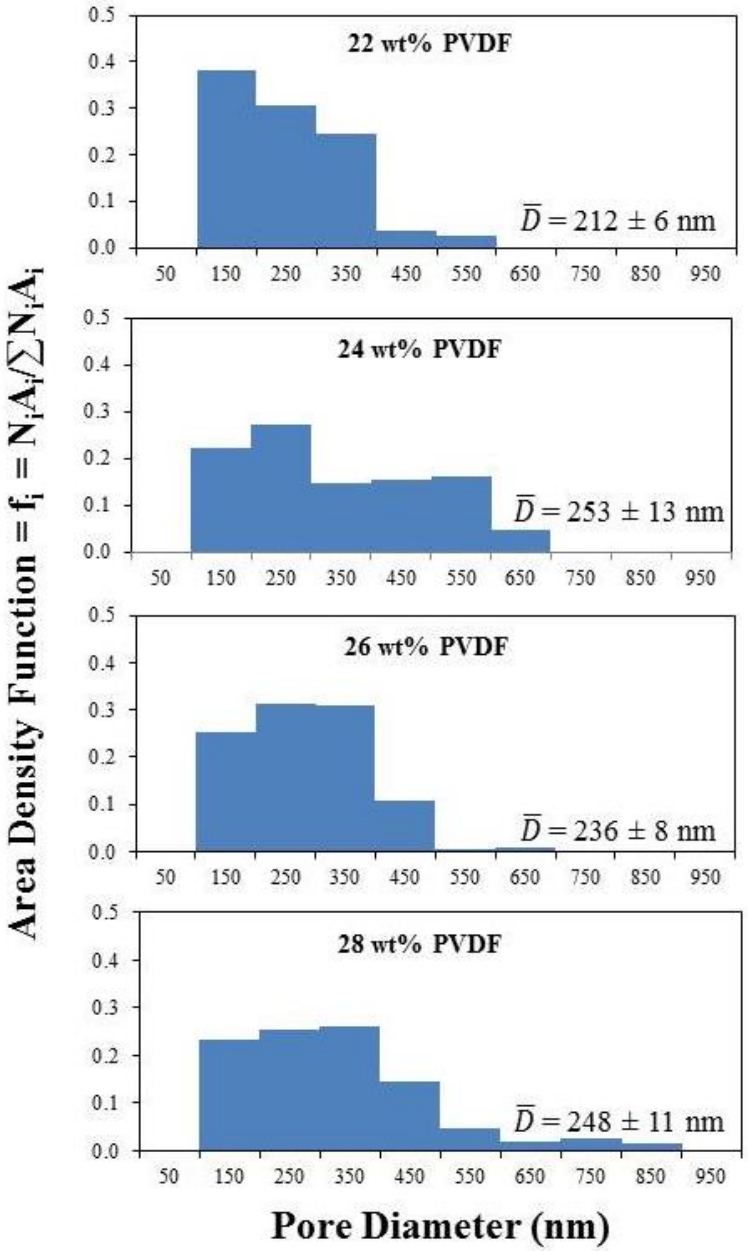

Fig. 4.9 Pore size distribution of PVDF membranes

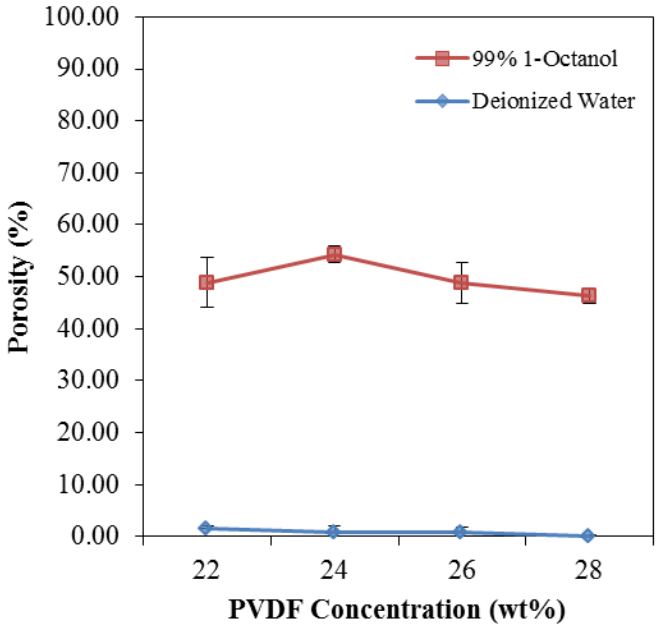

Fig. 4.10 Porosity of PVDF membranes

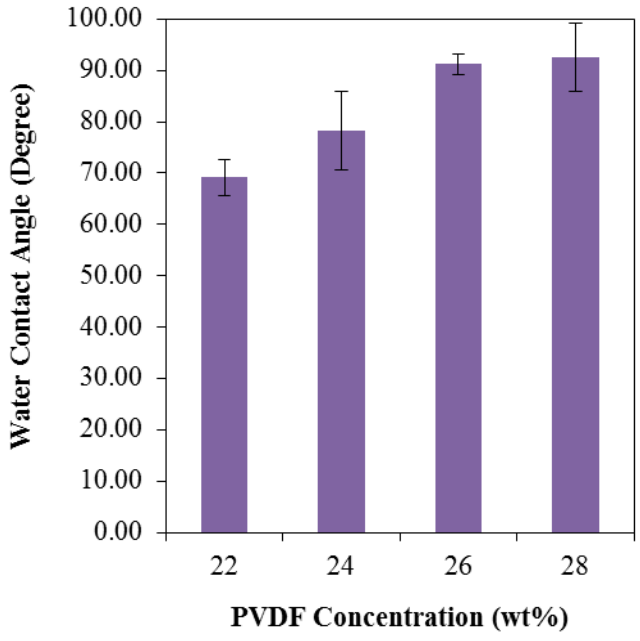

Fig. 4.11 Water contact angle of PVDF membranes

4.2.2 CNT/PVDF Composite Membrane

As mentioned earlier, suitable membrane for MGA should possess high porosity but small surface pore size. In this thesis, the PVDF membrane prepared from 26 % by weight was selected due to its high surface porosity and moderated pore sizes. More importantly, PVDF membrane with 26 % by weight was quite easy to be fabricated into a membrane sheet unlike PVDF membrane with 28 % by weight that was found too viscous and more difficult to get a uniform membrane.

PVDF membrane with 26 % by weight was composite with various CNT contents at 0.5, 1, 5, and 10 % by weight in PVDF. The structure of the prepared CNT/PVDF composite membranes was changed only slightly but the top surface was clearly affected by CNT loading as shown in **Fig. 4.12**. The whole membrane thickness of CNT/PVDF composite membranes was in a range of 139 – 204 μm, and the thin top layer of all CNT/PVDF composite membranes was less than 1 μm.

Surface porosity of the CNT/PVDF composite membranes was estimated and plotted in **Fig. 4.13**. It showed that surface porosity dropped when 0.5 % by weight of CNT loading was added and then rose again after increasing CNT loading. Pore size distribution was calculated and plotted in **Fig. 4.14**. The finger-liked middle layer was formed by the influence of non-solvent inflow and the sponge-liked bottom layer was formed by solvent imbibition as proposed in the previous section. From SEM images of cross-section (**Fig. 4.12**), the wall of macrovoids and sponge-liked layer were precipitated in nodule-liked. This nodule formation was expected to be due to the fast precipitation of polymer with the presence of CNTs. Due to its hydrophobicity, the addition of CNTs in the polymer solution could enhance the precipitation by enhancing solvent outflow from the polymer-rich phase [41]. More investigation in quaternary phase system should be determined to learn how phase separation occurred and to investigate surface porosity behavior.

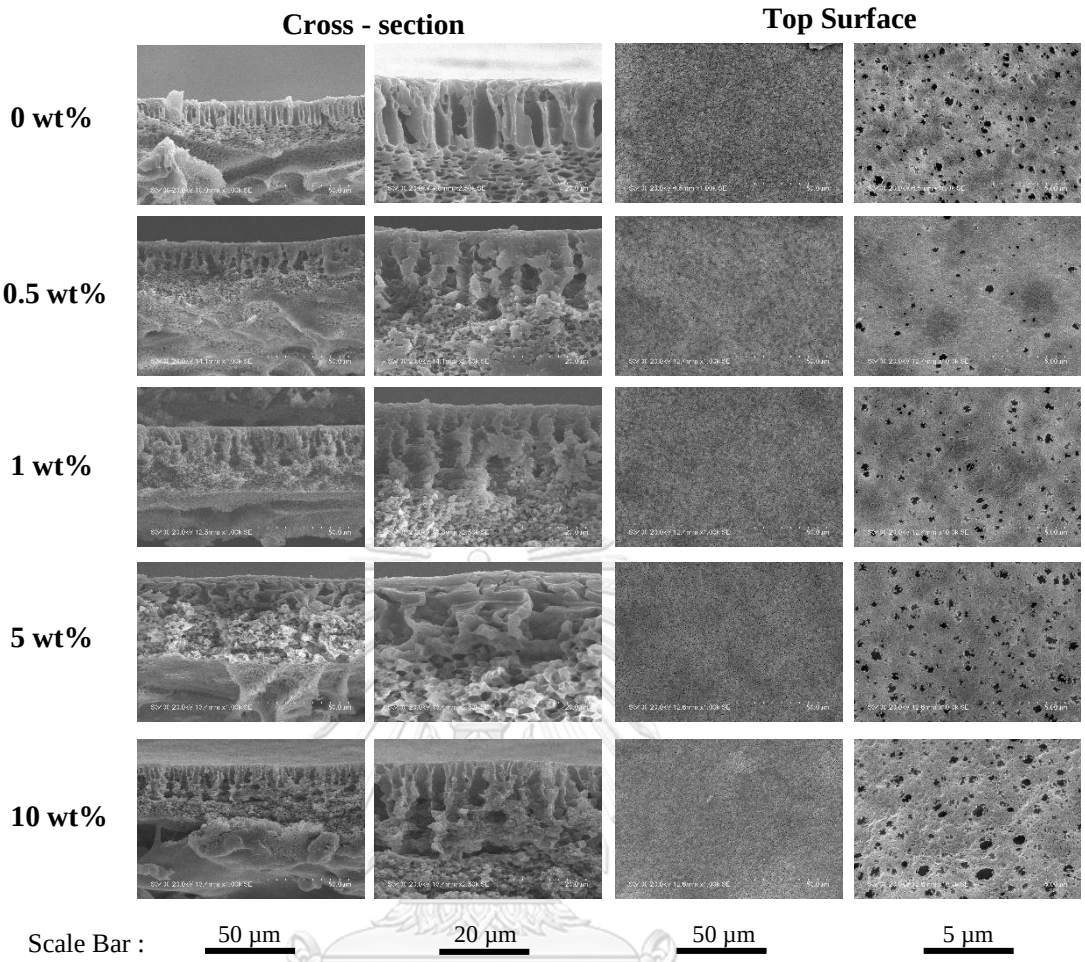

Fig. 4.12 SEM images of CNT/PVDF composite membranes

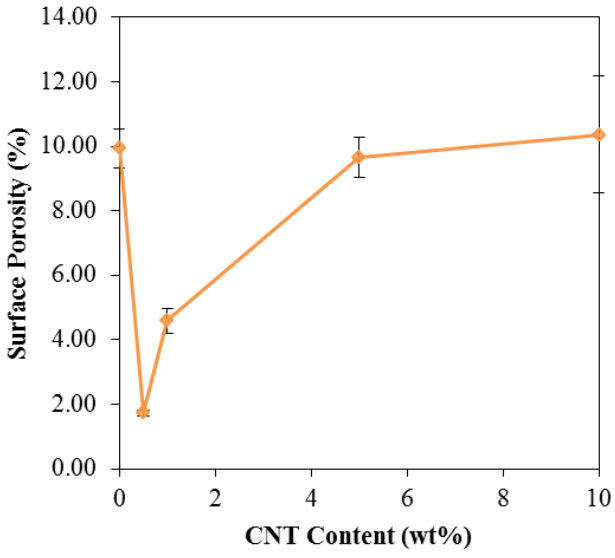

Fig. 4.13 Surface porosity of CNT/PVDF composite membranes

Porosity of CNT/PVDF composite membranes was measured and illustrated in **Fig. 4.15**. It showed that CNT/PVDF composite membranes were hydrophobic which could not absorb deionized water (0 - 2 %) in limited time. However, for 1-octanol, they could absorb and showed the narrow range of porosity by 42 - 49 % for all CNT/PVDF composite membranes.

Hydrophobicity of CNT/PVDF composite membranes was confirmed by water contact angle measurement as shown in **Fig. 4.16**. These results showed that CNT adding could slightly improve membrane hydrophobicity with the limited dose of CNT not over 5 % by weight. After CNT content reached 10 % by weight, the water contact angle dropped to 79˚ which was lower than the bare one. It is worth to mention that this water contact angle was affected by several parameters besides the effect of chemical composition, such as membrane morphology, surface roughness, and porosity. More systematic investigations were suggested. For instance, to eliminate the effect of membrane morphology on membrane hydrophobicity, a dense film from different composition of CNT and polymer should be fabricated to measure water contact angle.

The roughness of CNT/PVDF composite membrane surface was also determined to investigate its effect in membrane hydrophobicity. Two-dimension AFM micrographs were showed in **Fig. 4.17** and the roughness (R_a) of CNT/PVDF composite membrane surface was plotted in **Fig. 4.18**. The results showed that surface roughness average (R_a) was enhanced with an increase in CNT content. It is well-known that membrane hydrophobicity relates to membrane surface roughness, but it showed the different result in case of CNT/PVDF composite membrane with 10 % by weight of CNT loading. It might be due to its large surface porosity and pore size, leading to easily liquid penetration.

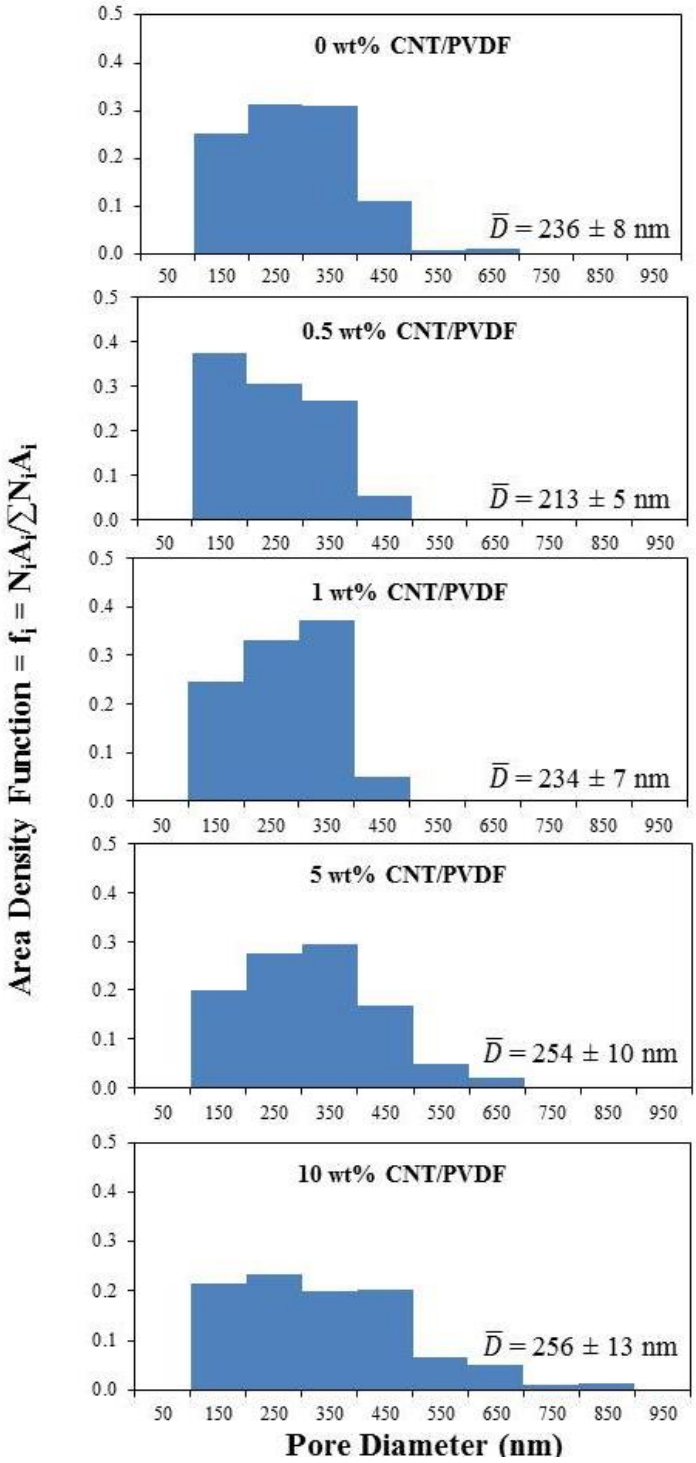

Fig. 4.14 Pore size distribution of CNT/PVDF composite membranes

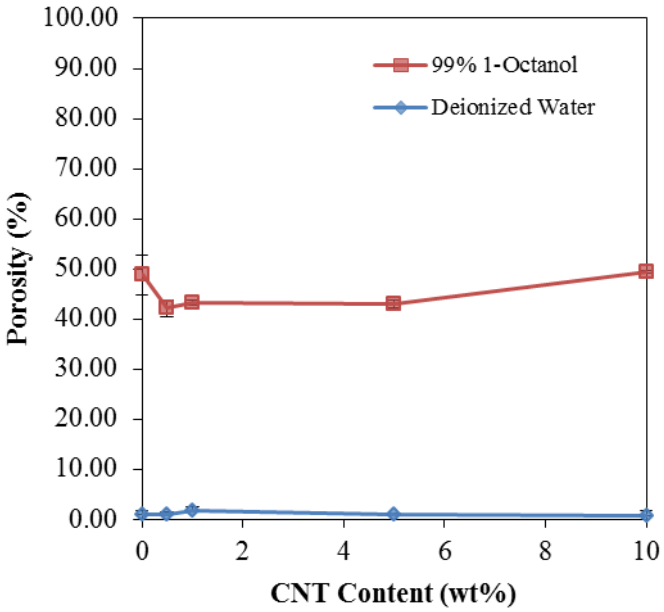

Fig. 4.15 Porosity of CNT/PVDF composite membranes

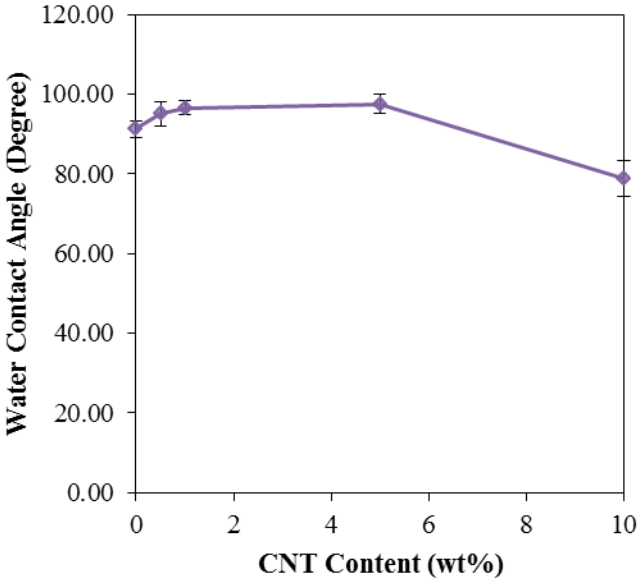

Fig. 4.16 Water contact angle of CNT/PVDF composite membranes

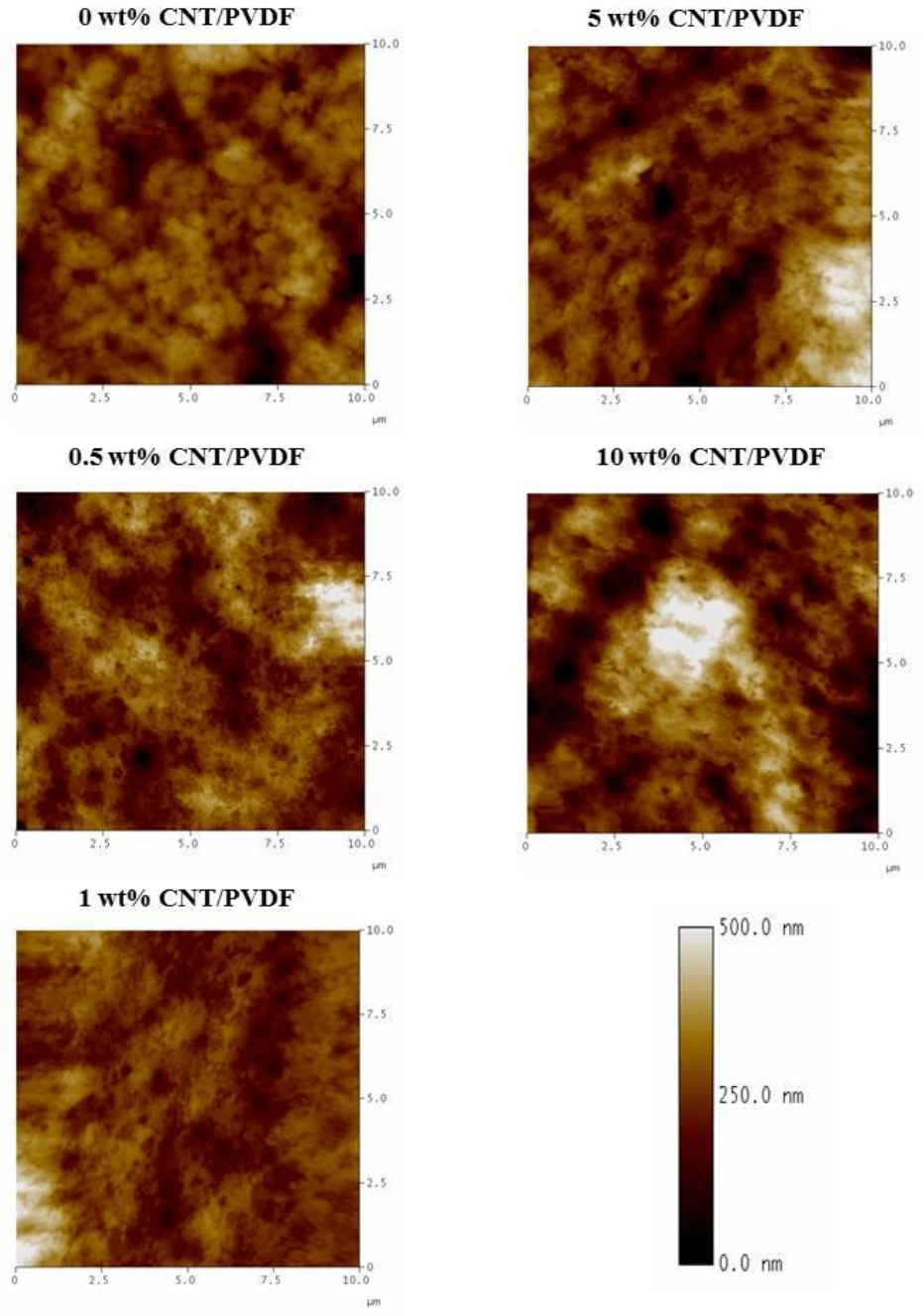

Fig. 4.17 Two-dimension AFM micrographs of CNT/PVDF composite membranes

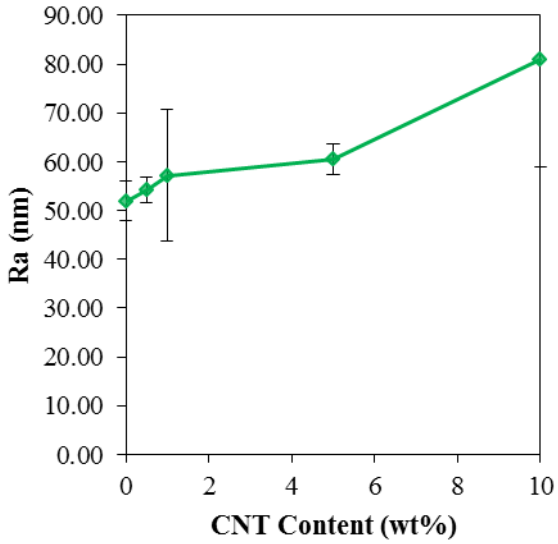

Fig. 4.18 Roughness average (R_a) of CNT/PVDF composite membranes

4.3 Comparison of Carbon Additives

To investigate the effect of carbonaceous filler types, carbon nanotubes (CNTs) and carbon black (CB) were composited with PAN or PVDF membrane at 5 % by weight in polymer.

4.3.1 Carbon Additives Properties

Carbon nanotubes and carbon black were characterized to investigate their pristine properties. SEM micrographs (see **Fig. 4.19**) and TEM micrographs (see **Fig. 4.20**) showed that CNTs were long tube shape and CB was sphere particles. Carbon particle size was measured by using an image processing and BET surface area (Belsorp-miniII, MicrotracBEL) was also measured, which were summarized in **Table 4.1**. CNT and CB were different in particle shape, size, and surface area. The aspect ratio of CNT was lower than 0.01 due to its elongated tube with small diameter, while the aspect ratio of CB was 0.82 which was closely spherical. Moreover, the surface area of CNT was 3.6 times higher than that of CB.

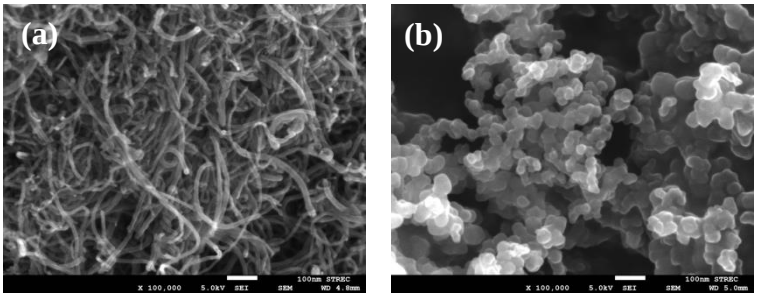

Fig. 4.19 SEM micrographs of (a) CNT and (b) CB

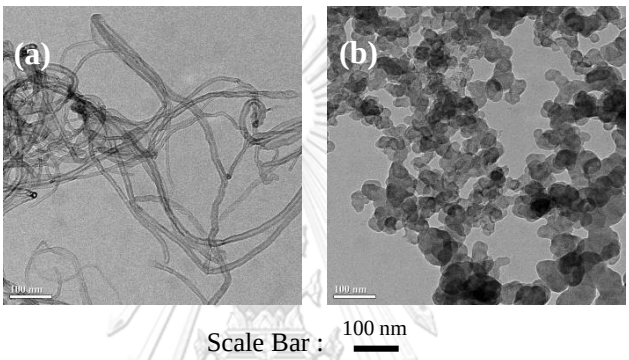

Fig. 4.20 TEM micrographs of (a) CNT and (b) CB

Table 4.1 Summary of carbon additives properties

Properties	**CNT**	**CB**
Average Particle Diameter (nm)	10 ± 3	38 ± 12
BET Surface area (m^2/g)	226.43	63.25

4.3.2 Carbon/PAN Composite Membrane

Morphology of the composite membranes from different carbonaceous fillers was found alike as shown in **Fig. 4.21**. Carbon/PAN composite membranes consisted of thin top layer and finger-liked pore structure as the same as that of bare PAN membrane. The top surface of CB/PAN composite membrane was dense but there was a crease on the surface unlike CNT/PAN composite membrane. Both CNTs and CB fillers insignificantly affected membrane morphology.

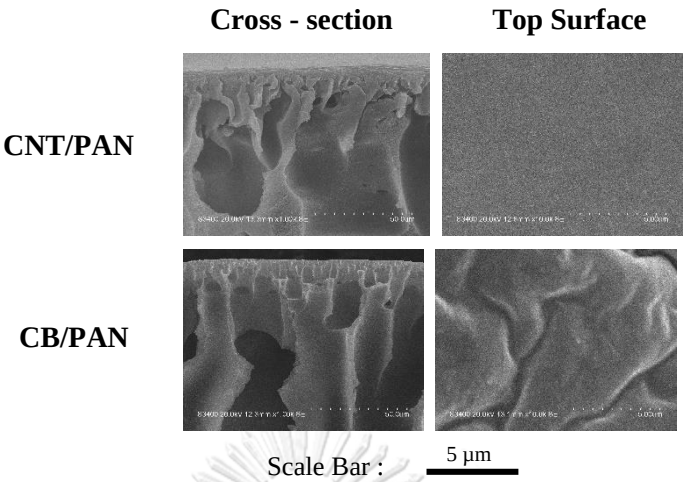

Fig. 4.21 SEM images of carbon/PAN composite membranes at 5 % by weight in polymer

Porosity of CNT/PAN and CB/PAN composite membranes was also compared in **Fig. 4.22**. The results revealed that the filler type has no significant influence on the membrane porosity. Water contact angle was also measured and showed that CNT/PAN and CB/PAN composite membranes were hydrophilic with water contact angle of 66.09 ± 2.54˚ and 63.61 ± 3.20˚, respectively.

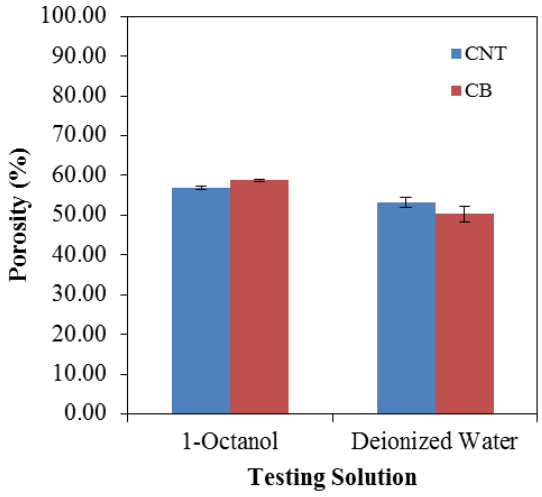

Fig. 4.22 Porosity of carbon/PAN composite membrane at 5 % by weight in polymer

Moreover, TGA analysis of PAN, composite CNT/PAN, and composite CB/PAN membranes showed that carbon addition did not significantly change thermal property of the bare and composite membranes, as shown in **Fig. 4.23**.

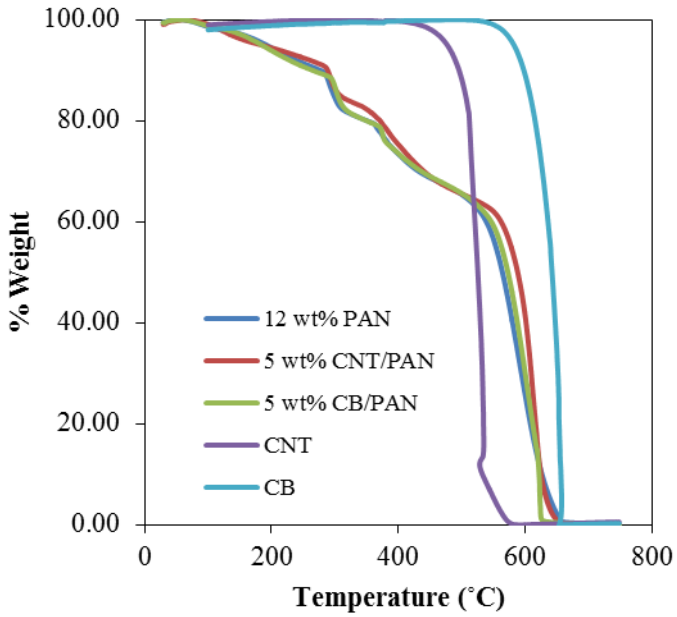

Fig. 4.23 TGA analysis of PAN, composite CNT/PAN, and composite CB/PAN membranes

4.3.3 Carbon/PVDF Composite Membrane

The main structure of carbon/PVDF composite membranes was consisted of three-layer structure; thin top layer, finger-liked middle layer, and sponge-liked bottom layer as same as that of bare PVDF membrane as shown in **Fig. 4.24**. The addition of different filler types resulted in a membrane with a difference in surface pore size. CB/PVDF composite membrane possessed smaller pore size than the CNT/PVDF composite membrane as it can be clearly noticed from **Fig. 4.25**. The pore size of CB/PVDF composite membrane was 207 ± 5 nm while the pore size of CNT/PVDF composite membrane was estimated to be 254 ± 10 nm. Surface porosity of the CNT/PVDF and CB/PVDF composite membranes was estimated to be 9.65 ± 0.63 % and 10.58 ± 0.31 %, respectively.

Porosity of CNT/PVDF and CB/PVDF composite membranes was also measured using 1-octanol and deionized water as the pore filling solution. The results

were compared in **Fig. 4.26**. Similar trend found in PAN series was observed in PVDF series; the different carbonaceous filler types had no effect on the membrane porosity.

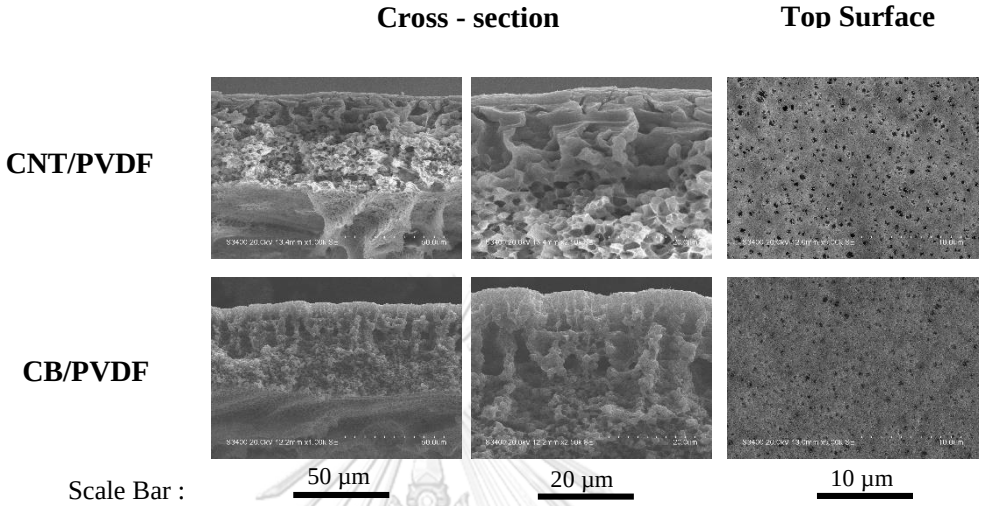

Fig. 4.24 SEM images of carbon/PVDF composite membranes at 5 % by weight in polymer

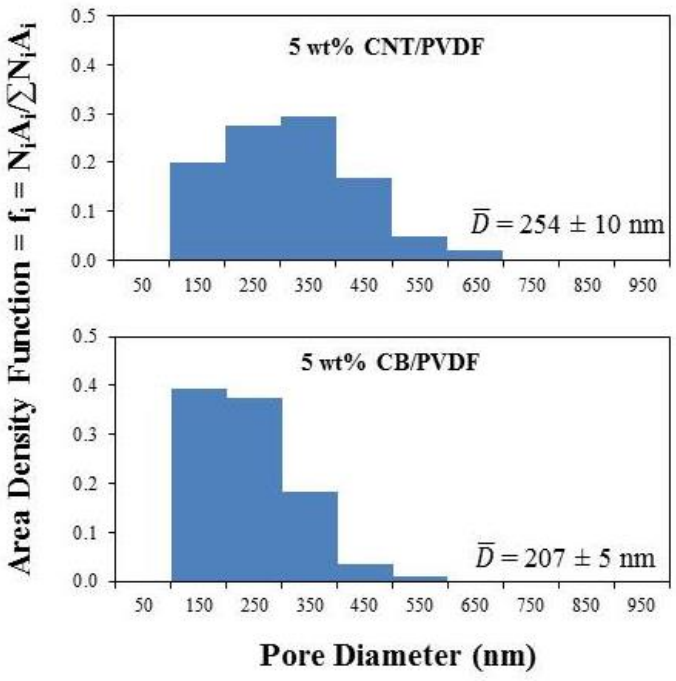

Fig. 4.25 Pore size distribution of carbon/PVDF composite membranes at 5 % by weight in polymer

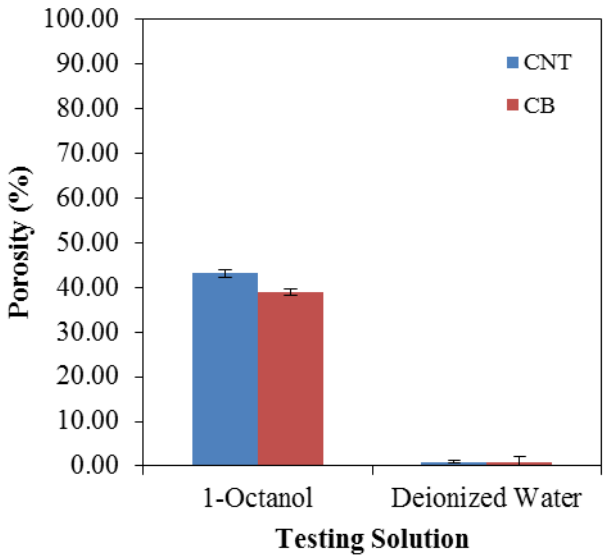

Fig. 4.26 Porosity of carbon/PVDF composite membranes at 5 % by weight in polymer

Water contact angle was also measured and showed that the results were 97.49˚ ± 2.34 for CNT/PVDF composite membrane and 88.70˚ ± 3.48 for CB/PVDF composite membrane, respectively. These results also showed that CNTs could improve PVDF membrane hydrophobicity better than CB could do.

Two-dimension AFM micrographs was also investigated and showed in **Fig. 4.27**. Roughness average of CNT/PVDF and CB/PVDF composite membranes was 60.49 ± 3.19 nm and 62.17 ± 5.58 nm, respectively, which was insignificantly different. This could imply that at the same loading CNT has stronger influence on membrane surface energy than CB.

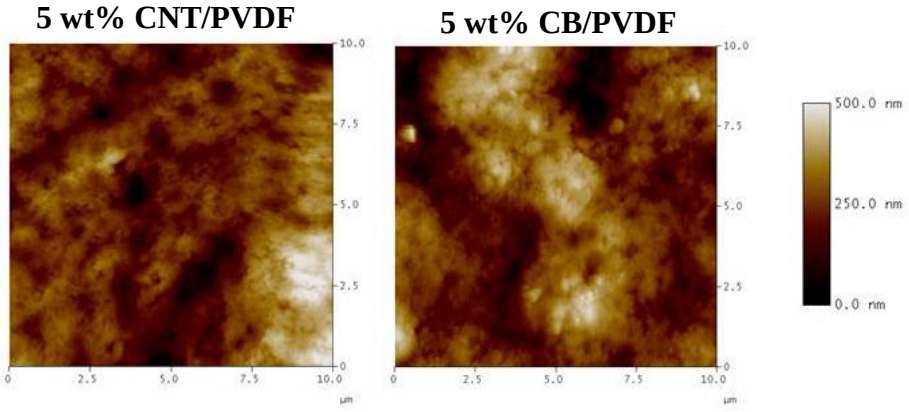

Fig. 4.27 Two-dimension AFM micrographs of carbon/PVDF composite membranes at 5 % by weight in polymer

Unlike the results from PAN series, the TGA analysis (**Fig. 4.28**) showed the change in weight reduction profile. CB/PVDF composite membrane could maintain the weight until 400 ˚C, while PVDF and composite CNT/PVDF membranes started to lose their weight from 80 ˚C. This result showed that CB could improve thermal resistance of the composite membrane, while CNT addition did not change thermal property of the composite membrane.

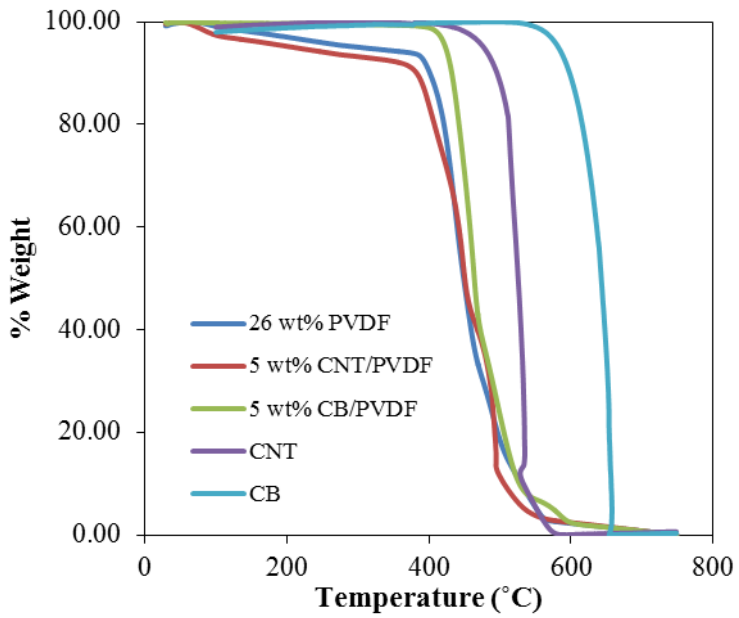

Fig. 4.28 TGA analysis of PVDF, composite CNT/PVDF, and composite CB/PVDF membranes

4.4 Performance Test

The fabricated membranes were tested in MGA system to investigate their performance in CO_2 capture. CO_2 absorption flux was determined. For membrane stability in a long-term operation, the changes in morphology and surface chemistry were investigated after contacting the fabricated membrane with 3 M MEA for 30 days.

Typical experiments of CO_2 capture were conducted in MGA system using the fabricated membranes based on both PAN and PVDF. Moreover, CB/PVDF composite membrane was also compared with bare PVDF and composite CNT/PVDF membrane to investigate the effects of carbonaceous additive types on CO_2 absorption.

4.4.1 PAN and CNT/PAN Membranes

The fabricated PAN and composite CNT/PAN membranes were tested in MGA system. After 30 min of the operation, both bare and composite membranes were wetted. The droplets of liquid absorbent (3 M MEA) were observed at the gas-side of the membrane. In the case of CB/PAN composite membrane, the absorbent droplets were also found at the gas-side of the membrane. This result was expected as bare and carbon composite PAN membranes were not suitable for MGA system due to its hydrophilicity. As it was concluded from the previous section, CNT and CB addition could not enhance hydrophobicity of the PAN membrane.

4.4.2 PVDF and CNT/PVDF Membranes

CO_2 capture was successfully achieved for PVDF and composite CNT/PVDF membranes in MGA system. The CO_2 absorption flux was calculated and plotted in **Fig. 4.29**.

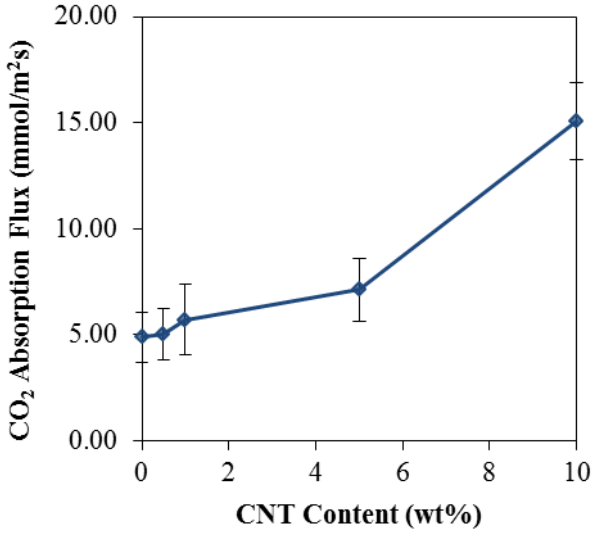

Fig. 4.29 CO_2 absorption flux of CNT/PVDF membranes

It showed that CNT/PVDF composite membranes provided a higher CO_2 absorption flux than that of the bare one, even though its surface porosity was lower in the case of 0.5 - 1 % by weight of CNT loading. Membrane hydrophobicity could play a role in less partially membrane wetting, leading to an enhanced CO_2 absorption performance in the composite membranes. In the case of 5 wt% CNT/PVDF composite membrane, CO_2 absorption flux could reach 7.12 mmol/m^2s with 46 % improvement compared to the bare one. Even though surface porosity of 26 wt% PVDF membrane and 5 wt% CNT/PVDF composite membrane was relatively equal (see **Fig. 4.13**), CO_2 absorption flux of CNT/PVDF composite membrane with 5 % by weight of CNT loading was much larger than that of the bare one due to its more hydrophobicity. In the case of 10 wt% CNT/PVDF composite membrane, CO_2 absorption flux could reach 15.1 mmol/m^2s, which was 209 % increment compared to the bare one. In this case, CNT/PVDF composite membrane with 10 % by weight of CNT loading possessed highest surface porosity, leading to higher effective membrane area. However, liquid penetration could occur and damaged membrane in a longer operation time.

4.4.3 Effect of Carbonaceous Filler Types on Membrane Performance

Bare PVDF membrane and its composite membrane with 5 % by weight of CNT and 5 % by weight of CB were also tested in MGA system. Their performances were compared in **Fig. 4.30**. The results showed that both CNT/PVDF and CB/PVDF composite membranes provided higher CO_2 absorption flux than that of the bare one due to their higher membrane hydrophobicity.

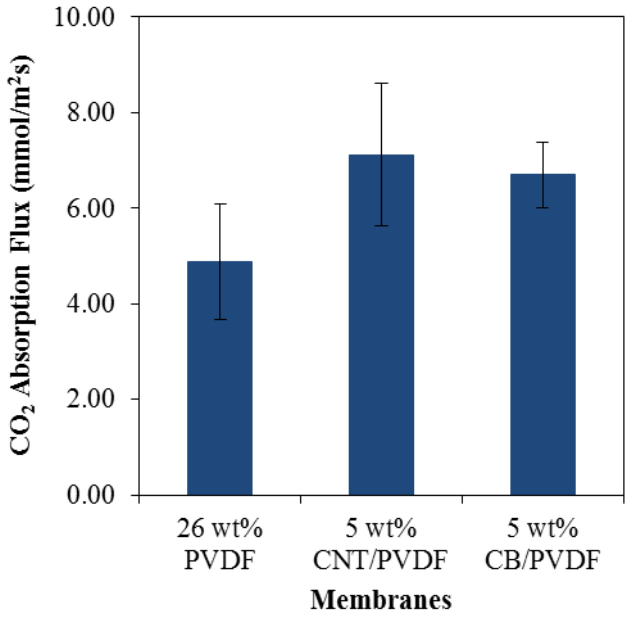

Fig. 4.30 CO_2 absorption flux of the bare PVDF, composite CNT/PVDF, and composite CB/PVDF membranes

The potential of the fabricated membranes for long-term operation was also investigated. The membranes were contacted with 3 M MEA for 30 days and then their morphology and surface chemicals were investigated. SEM micrographs (see **Fig. 4.31**) showed that surface porosity of all membranes was reduced after contacted with 3 M MEA for 10 days. Pore size distribution changed and average membrane pore size was also reduced, which were confirmed in **Fig. 4.32**. Fouling was also found on the membrane surface after contacted with 3 M MEA in 26 wt% PVDF membrane and 5 wt% CNT/PVDF composite membrane.

For the bare PVDF membrane, some membrane pores were enlarged by liquid penetration and the membrane surface were cracked after being used for 30 days.

CNT/PVDF and CB/PVDF composite membranes seemed to get smaller after 30 days of MEA exposure. The reasons for this unexpected pore shrinkage remained unclear. It might be due to solvent-shrinkage, leading to membrane swelling [42].

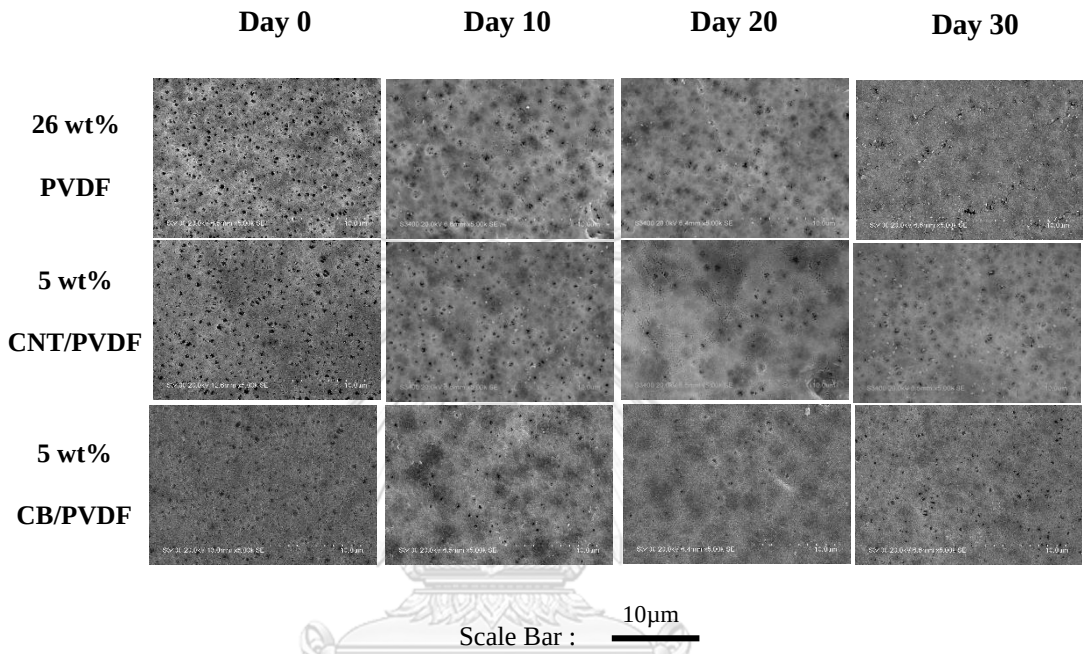

Fig. 4.31 SEM micrographs of 26 wt% PVDF, 5 wt% CNT/PVDF, and 5 wt% CB/PVDF membranes after contacted with 3 M MEA at day 0, 10, 20, and 30

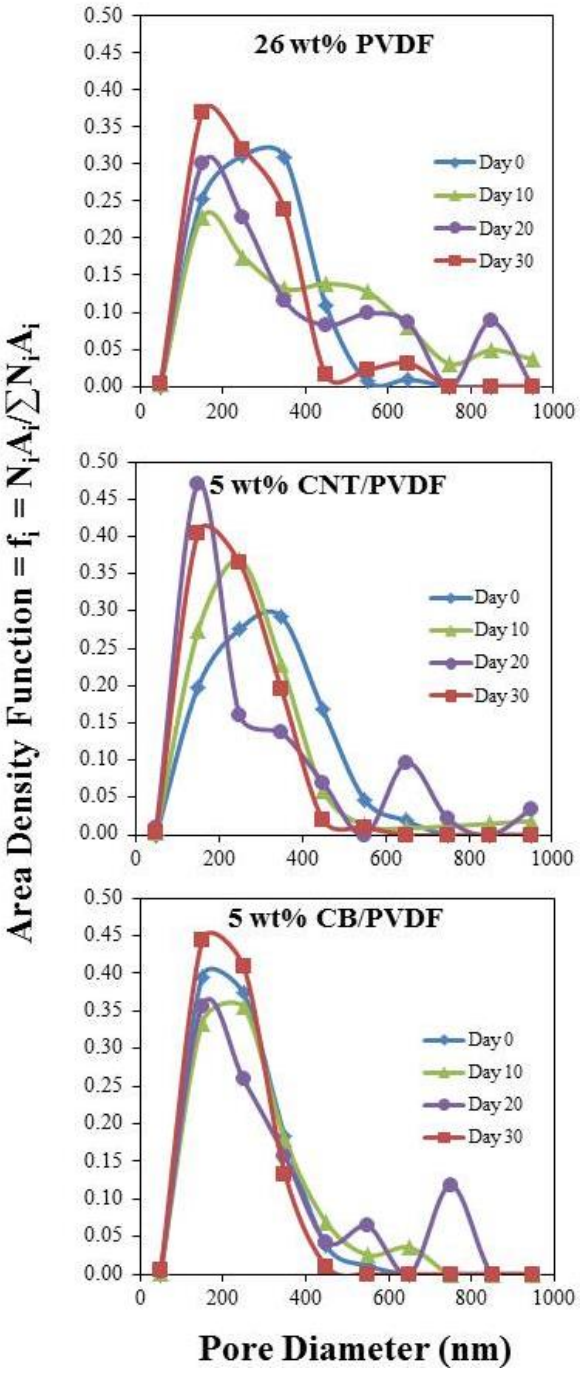

Fig. 4.32 Pore size distribution of 26 wt% PVDF, 5 wt% CNT/PVDF, and 5 wt% CB/PVDF membranes after contacted with 3 M MEA at day 0, 10, 20, and 30

Membrane surface chemicals were also investigated. There was no chemical change on the membrane surface after being contacted with 3 M MEA as shown in **Fig 4.33**. The main peak that was found at wavenumbers of 2800-2900 cm^{-1} was the peak of C-H bond, and there was no other significant peak in the region.

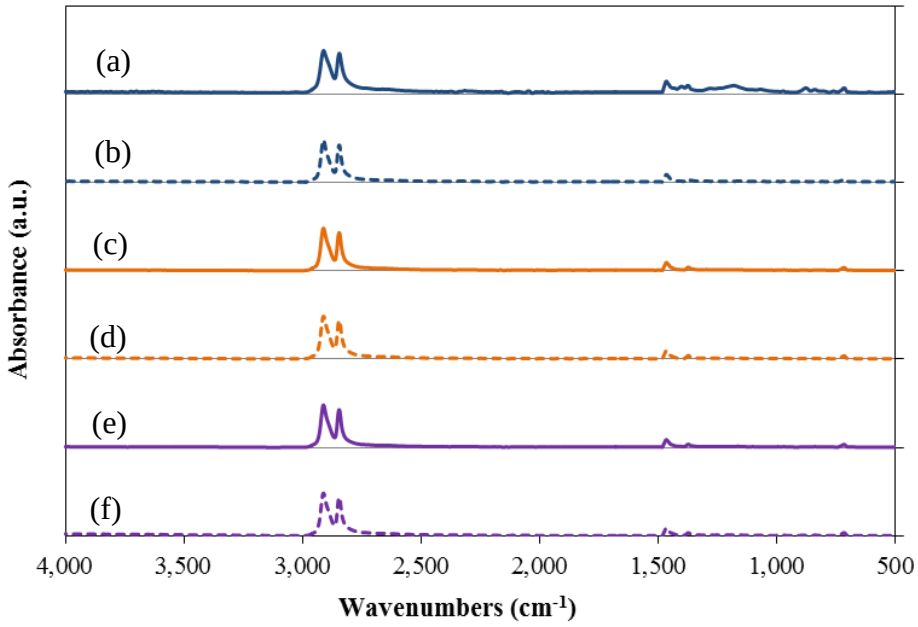

Fig. 4.33 FTIR spectrum of (a) 26 wt% PVDF – Day 0, (b) 26 wt% PVDF – Day 30, (c) 5 wt% CNT/PVDF – Day 0, (d) 5 wt% CNT/PVDF – Day 30, (e) 5 wt% CB/PVDF – Day 0, and (f) 5 wt% CB/PVDF – Day 30

For long-term stability, the composite PVDF membrane of CNT and CB possessed the ability to use in MGA system. Though the composite membranes were slightly swelled after being exposed to the absorbent for 30 days, their surface did not change due to their chemical resistance. CNT and CB addition improved both wetting resistance of the PVDF membrane and CO_2 absorption performance in MGA system.

5. Conclusion

Two types of polymer, namely PAN and PVDF, were used to fabricate bare and composite membranes for CO_2 capture in MGA system. The effects of CNT as filler on the resultant composite membranes were summarized below.

5.1 PAN and CNT/PAN

PAN membranes consisted of finger-liked porous bottom layer and thin top dense layer. CNT addition (0.5 – 10 % by weight in PAN) exerted insignificant effect on membrane morphology and membrane hydrophobicity. As a result, PAN based membranes could not resist liquid penetration and got wet after used in MGA system for only 30 min.

5.2 PVDF and CNT/PVDF

Typical PVDF membranes consisted of 3-layer structure; thin top layer, finger-liked middle layer, and sponge-liked bottom layer. The membrane surface was porous and exhibited hydrophobic property with contact angle of 91˚. CNT addition affected membrane surface porosity. Surface porosity dropped when 0.5 % by weight of CNT loading were added but increased with a further increase in CNT loading. CNT loading also affected membrane pore size distribution. Membrane pore size increased with an increase in CNT loading. Water contact angle became higher with an increase in CNT loading, except in the composite membrane with 10 % by weight of CNT loading. Water contact angle of CNT/PVDF composite membrane with 10 % by weight of CNT loading dropped due to its large pore size, leading to higher liquid penetration.

When the fabricated membranes were tested in MGA system, CNT/PVDF composite membrane with 10 % by weight of CNT loading showed the highest CO_2 absorption flux at 15.1 mmol/m^2s, but its large pore size could result in higher liquid penetration and damaged the membrane in a longer operation. Thus, CNT/PVDF composite membrane with 5 % by weight of CNT loading was considered to be the best condition for MGA system, which possessed highest water contact angle and

uniform pore size distribution with small pore size (CO_2 absorption flux = 7.12 mol/m^2s).

5.3 Effect of Carbonaceous Filler Type

Two types of fillers, namely CNTs and CB, were compared by dispersing in PVDF matrix at 5 % by weight of carbon loading. The structure of CNT/PVDF and CB/PVDF composite membranes were alike. The CB/PVDF composite membrane exerted smaller surface pore size than that of CNT/PVDF composite membrane, while water contact angle of CNT/PVDF composite membrane was higher than that of CB/PVDF composite membrane.

CO_2 absorption flux of CNT/PVDF and CB/PVDF composite membranes was also higher than that of the bare one, resulted from higher hydrophobicity and surface porosity. Pore size reduction was found in CNT/PVDF and CB/PVDF composite membranes after contacted with 3 M MEA for 30 days, resulted from membrane swelling due to solvent penetration. In case of bare PVDF membrane with 26 % by weight, surface crack and enlarged surface pore were observed. Both CNT and CB fillers were proved to enhance hydrophobicity and wetting resistance of the composite membranes and would enhance their stability in a long-term operation. To further investigate the effect of different carbon additive particles on membrane morphology, more type of carbon particles with different aspect ratio should be used to fabricate composite membrane.

5.4 Recommendation

In this thesis, CNT/PVDF composite membrane was successfully fabricated to use in MGA system for CO_2 capture. Some composite membrane showed the good performance and stability. However, all composite membrane was fabricated in flat sheet which would lead to a limitation of lab-scale MGA application due to its low surface area per unit volume. The hollow fiber membrane would be suggested to form CNT/PVDF composite membrane and investigated their properties. Also, operational parameter effects should be investigated for more feasibility in CO_2 capture from flue gas, such as gas and liquid flow rate, CO_2 inlet concentration, and operating temperature.

Moreover, CB/PVDF composite membrane also showed good characteristics in this thesis. More investigation in CB/PVDF composite membrane for MGA application would be suggested.

REFERENCES

[1] J. C. M. Pires, F. G. Martins, M. C. M. Alvim-Ferraz, and M. Simões, "Recent developments on carbon capture and storage: An overview," *Chemical Engineering Research and Design*, vol. 89, pp. 1446-1460, 2011.

[2] M. K. Mondal, H. K. Balsora, and P. Varshney, "Progress and trends in CO2 capture/separation technologies: A review," *Energy*, vol. 46, pp. 431-441, 2012.

[3] D. Y. C. Leung, G. Caramanna, and M. M. Maroto-Valer, "An overview of current status of carbon dioxide capture and storage technologies," *Renewable and Sustainable Energy Reviews*, vol. 39, pp. 426-443, 2014.

[4] S. Rajabzadeh, S. Yoshimoto, M. Teramoto, M. Al-Marzouqi, and H. Matsuyama, "CO2 absorption by using PVDF hollow fiber membrane contactors with various membrane structures," *Separation and Purification Technology*, vol. 69, pp. 210-220, 2009.

[5] J.-L. Li and B.-H. Chen, "Review of CO2 absorption using chemical solvents in hollow fiber membrane contactors," *Separation and Purification Technology*, vol. 41, pp. 109-122, 2005.

[6] S. Mosadegh-Sedghi, D. Rodrigue, J. Brisson, and M. C. Iliuta, "Wetting phenomenon in membrane contactors – Causes and prevention," *Journal of Membrane Science*, vol. 452, pp. 332-353, 2014.

[7] S. Rajabzadeh, S. Yoshimoto, M. Teramoto, M. Al-Marzouqi, Y. Ohmukai, T. Maruyama, *et al.*, "Effect of membrane structure on gas absorption performance and long-term stability of membrane contactors," *Separation and Purification Technology*, vol. 108, pp. 65-73, 2013.

[8] W. Rongwong, R. Jiraratananon, and S. Atchariyawut, "Experimental study on membrane wetting in gas–liquid membrane contacting process for CO2 absorption by single and mixed absorbents," *Separation and Purification Technology*, vol. 69, pp. 118-125, 2009.

[9] A. L. Ahmad and W. K. W. Ramli, "Hydrophobic PVDF membrane via two-stage soft coagulation bath system for Membrane Gas Absorption of CO2," *Separation and Purification Technology*, vol. 103, pp. 230-240, 2013.

[10] A. L. Ahmad, W. K. W. Ramli, W. J. N. Fernando, and W. R. W. Daud, "Effect of ethanol concentration in water coagulation bath on pore geometry of PVDF membrane for Membrane Gas Absorption application in CO2 removal," *Separation and Purification Technology*, vol. 88, pp. 11-18, 2012.

[11] Y. Zhang, R. Wang, L. Zhang, and A. G. Fane, "Novel single-step hydrophobic modification of polymeric hollow fiber membranes containing imide groups: Its potential for membrane contactor application," *Separation and Purification Technology*, vol. 101, pp. 76-84, 2012.

[12] Y. Zhang and R. Wang, "Fabrication of novel polyetherimide-fluorinated silica organic–inorganic composite hollow fiber membranes intended for membrane contactor application," *Journal of Membrane Science*, vol. 443, pp. 170-180, 2013.

[13] Y. Zhang and R. Wang, "Novel method for incorporating hydrophobic silica nanoparticles on polyetherimide hollow fiber membranes for CO2 absorption

in a gas–liquid membrane contactor," *Journal of Membrane Science,* vol. 452, pp. 379-389, 2014.

[14] A. Mansourizadeh, Z. Aslmahdavi, A. F. Ismail, and T. Matsuura, "Blend polyvinylidene fluoride/surface modifying macromolecule hollow fiber membrane contactors for CO2 absorption," *International Journal of Greenhouse Gas Control,* vol. 26, pp. 83-92, 2014.

[15] M. Rahbari-Sisakht, A. F. Ismail, D. Rana, and T. Matsuura, "Effect of novel surface modifying macromolecules on morphology and performance of Polysulfone hollow fiber membrane contactor for CO2 absorption," *Separation and Purification Technology,* vol. 99, pp. 61-68, 2012.

[16] M. Rahbari-Sisakht, A. F. Ismail, D. Rana, T. Matsuura, and D. Emadzadeh, "Effect of SMM concentration on morphology and performance of surface modified PVDF hollow fiber membrane contactor for CO2 absorption," *Separation and Purification Technology,* vol. 116, pp. 67-72, 2013.

[17] M. Rahbari-Sisakht, A. F. Ismail, D. Rana, and T. Matsuura, "A novel surface modified polyvinylidene fluoride hollow fiber membrane contactor for CO2 absorption," *Journal of Membrane Science,* vol. 415-416, pp. 221-228, 2012.

[18] M. Rezaei, A. F. Ismail, G. Bakeri, S. A. Hashemifard, and T. Matsuura, "Effect of general montmorillonite and Cloisite 15A on structural parameters and performance of mixed matrix membranes contactor for CO2 absorption," *Chemical Engineering Journal,* vol. 260, pp. 875-885, 2015.

[19] M. Rezaei DashtArzhandi, A. F. Ismail, T. Matsuura, B. C. Ng, and M. S. Abdullah, "Fabrication and characterization of porous polyetherimide/montmorillonite hollow fiber mixed matrix membranes for CO2 absorption via membrane contactor," *Chemical Engineering Journal,* vol. 269, pp. 51-59, 2015.

[20] M. Rezaei, A. F. Ismail, S. A. Hashemifard, and T. Matsuura, "Preparation and characterization of PVDF-montmorillonite mixed matrix hollow fiber membrane for gas–liquid contacting process," *Chemical Engineering Research and Design,* vol. 92, pp. 2449-2460, 11// 2014.

[21] B. K. Kaushik and M. K. Majumder, "Carbon Nanotube: Properties and Applications," pp. 17-37, 2015.

[22] O. Breuer and U. Sundararaj, "Big returns from small fibers: A review of polymer/carbon nanotube composites," *Polymer Composites,* vol. 25, pp. 630-645, 2004.

[23] A. Sharma, B. Tripathi, and Y. K. Vijay, "Dramatic Improvement in properties of magnetically aligned CNT/polymer nanocomposites," *Journal of Membrane Science,* vol. 361, pp. 89-95, 2010.

[24] H. Cong, J. Zhang, M. Radosz, and Y. Shen, "Carbon nanotube composite membranes of brominated poly(2,6-diphenyl-1,4-phenylene oxide) for gas separation," *Journal of Membrane Science,* vol. 294, pp. 178-185, 2007.

[25] S. G. Ding, X. Q. Cheng, Z. X. Jiang, Y. P. Bai, and L. Shao, "Pore morphology control and hydrophilicity of polyacrylonitrile ultrafiltration membranes," *Journal of Applied Polymer Science,* vol. 132, pp. n/a-n/a, 2015.

[26] G. R. Guillen, Y. Pan, M. Li, and E. M. V. Hoek, "Preparation and Characterization of Membranes Formed by Nonsolvent Induced Phase

Separation: A Review," *Industrial & Engineering Chemistry Research*, vol. 50, pp. 3798-3817, 2011.

[27] R. W. Baker, "Membrane Transport Theory," in *Membrane Technology and Applications*, ed: John Wiley & Sons, Ltd, 2004, pp. 15-87.

[28] S. H. Lin, K. L. Tung, H. W. Chang, and K. R. Lee, "Influence of fluorocarbon flat-membrane hydrophobicity on carbon dioxide recovery," *Chemosphere*, vol. 75, pp. 1410-6, Jun 2009.

[29] M. H. Al-Marzouqi, M. H. El-Naas, S. A. M. Marzouk, M. A. Al-Zarooni, N. Abdullatif, and R. Faiz, "Modeling of CO2 absorption in membrane contactors," *Separation and Purification Technology*, vol. 59, pp. 286-293, 2008.

[30] A. Mansourizadeh, A. F. Ismail, and T. Matsuura, "Effect of operating conditions on the physical and chemical CO2 absorption through the PVDF hollow fiber membrane contactor," *Journal of Membrane Science*, vol. 353, pp. 192-200, 2010.

[31] Y. Lv, X. Yu, J. Jia, S.-T. Tu, J. Yan, and E. Dahlquist, "Fabrication and characterization of superhydrophobic polypropylene hollow fiber membranes for carbon dioxide absorption," *Applied Energy*, vol. 90, pp. 167-174, 2012.

[32] L. Wang, Z. Zhang, B. Zhao, H. Zhang, X. Lu, and Q. Yang, "Effect of long-term operation on the performance of polypropylene and polyvinylidene fluoride membrane contactors for CO2 absorption," *Separation and Purification Technology*, vol. 116, pp. 300-306, 2013.

[33] B. P. Ter Meulen, "Basic Principles of Membrane Technology. M. Mulder. Kluwer, Dordrecht, 1991. 372 pp., Hardbound Dfl. 200.00/£69.00. Paperback Dfl. 70.00/£24.00. ISBN 0-7923-0978-2 Hardbound. ISBN 0-7923-0979-2 Paperback," *Recueil des Travaux Chimiques des Pays-Bas*, vol. 111, pp. 458-458, 1992.

[34] C. A. Smolders, A. J. Reuvers, R. M. Boom, and I. M. Wienk, "Microstructures in phase-inversion membranes. Part 1. Formation of macrovoids," *Journal of Membrane Science*, vol. 73, pp. 259-275, 1992/10/09 1992.

[35] H. Strathmann and K. Kock, "The formation mechanism of phase inversion membranes," *Desalination*, vol. 21, pp. 241-255, 1977/09/01 1977.

[36] P. van de Witte, P. J. Dijkstra, J. W. A. van den Berg, and J. Feijen, "Phase separation processes in polymer solutions in relation to membrane formation," *Journal of Membrane Science*, vol. 117, pp. 1-31, 1996/08/21 1996.

[37] J.-Y. Lai, F.-C. Lin, T.-T. Wu, and D.-M. Wang, "On the formation of macrovoids in PMMA membranes," *Journal of Membrane Science*, vol. 155, pp. 31-43, 3/31/ 1999.

[38] D.-M. Wang, F.-C. Lin, T.-T. Wu, and J.-Y. Lai, "Formation mechanism of the macrovoids induced by surfactant additives," *Journal of Membrane Science*, vol. 142, pp. 191-204, 5/13/ 1998.

[39] T.-H. Young and L.-W. Chen, "Pore formation mechanism of membranes from phase inversion process," *Desalination*, vol. 103, pp. 233-247, 1995/12/01 1995.

[40] J.-H. Kim and K.-H. Lee, "Effect of PEG additive on membrane formation by phase inversion," *Journal of Membrane Science,* vol. 138, pp. 153-163, 1998/01/21 1998.

[41] X. Wu, B. Zhao, L. Wang, Z. Zhang, H. Zhang, X. Zhao, *et al.*, "Hydrophobic PVDF/graphene hybrid membrane for CO 2 absorption in membrane contactor," *Journal of Membrane Science,* vol. 520, pp. 120-129, 2016.

[42] E. J. Vriezekolk, A. J. B. Kemperman, M. Gironès, W. M. de Vos, and K. Nijmeijer, "A solvent-shrinkage method for producing polymeric microsieves with sub-micron size pores," *Journal of Membrane Science,* vol. 446, pp. 10-18, 2013.

APPENDIX

Appendix A : Image Processing

A1 Membrane Surface Porosity and Pore Size Distribution

Membrane pore size distribution was measured and calculated by using an image processing, ImageJ 1.50i, National Institutes of Health, USA, following the steps below.

1) Selected the SEM micrograph and opened with the program
2) Set the scale according to the scale bar in micrograph (Analyze >> Set Scale)

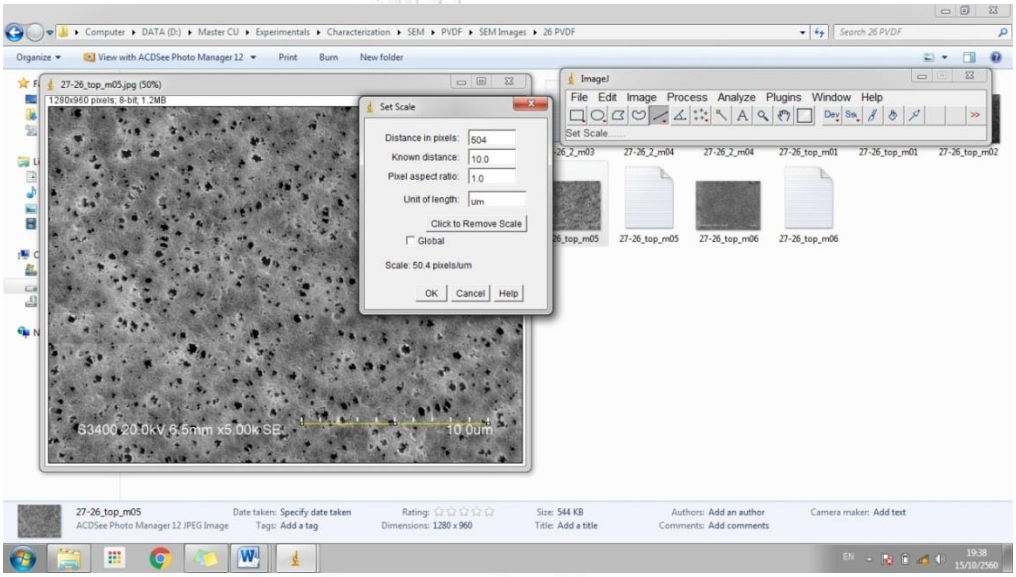

3) Adjusted threshold to fitly fill the pore area (Image >> Adjust >> Threshold)

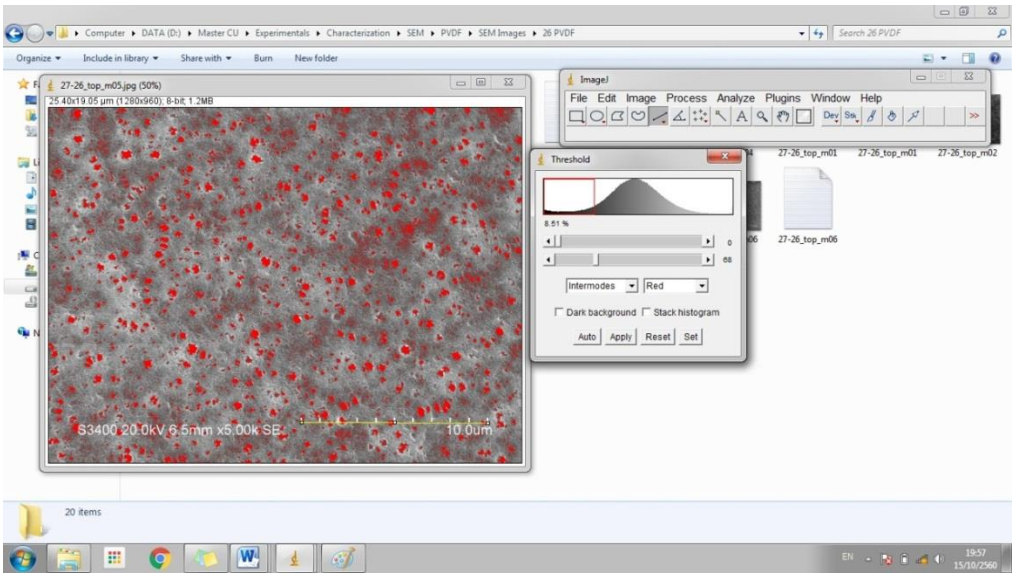

4) Measured the filled area to determine membrane surface porosity (Analyze >> Measure)

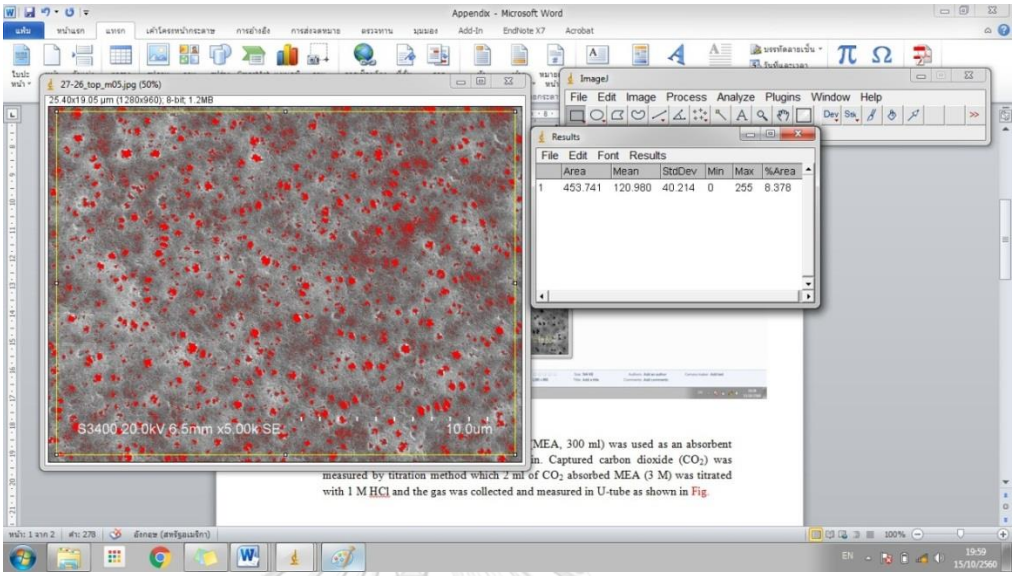

5) Analyzed membrane pore size (Analyze >> Analyze Particles)

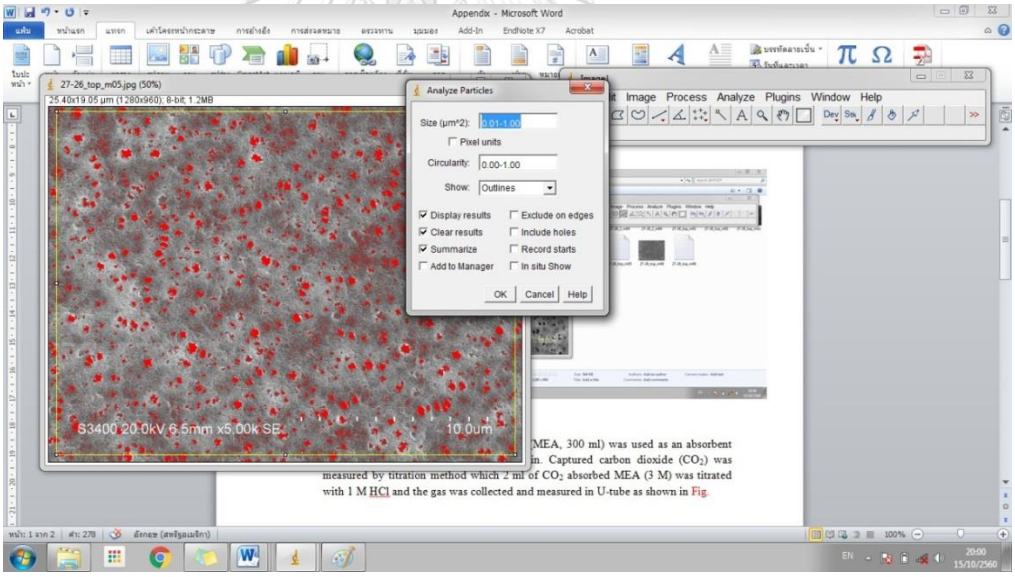

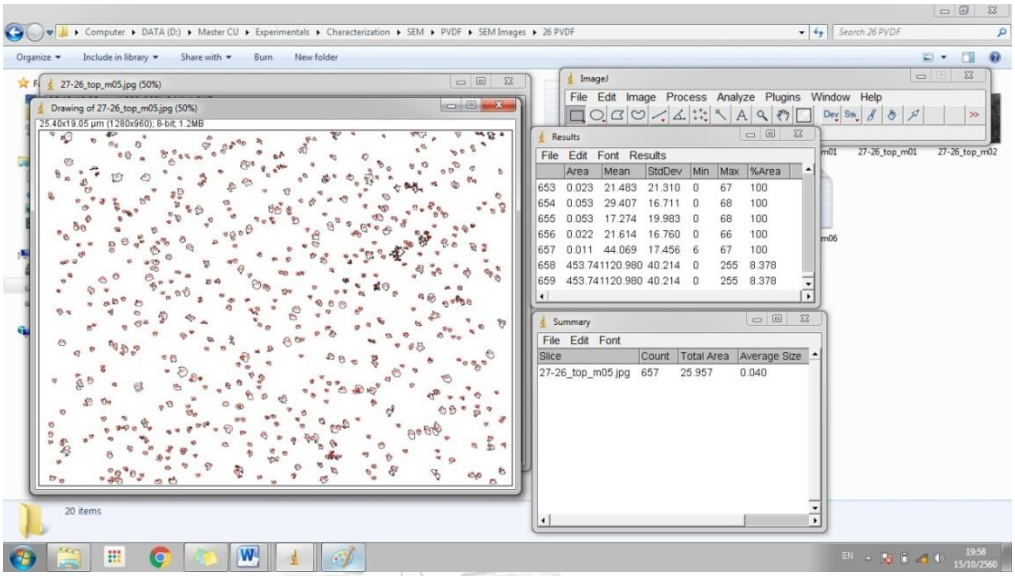

6) Saved the data to calculate pore size distribution by using area base

A2 Carbon Particle Size

TEM micrographs of carbon particle were used to measured their size by using an image processing, SemAfore 5.21, JEOL, Sweden. After set the scale according to the scale in the micrograph (in μm), "measure mode" was used to measure particle size as shown in **Fig. A2.1**. The measured particle size was collected and calculated.

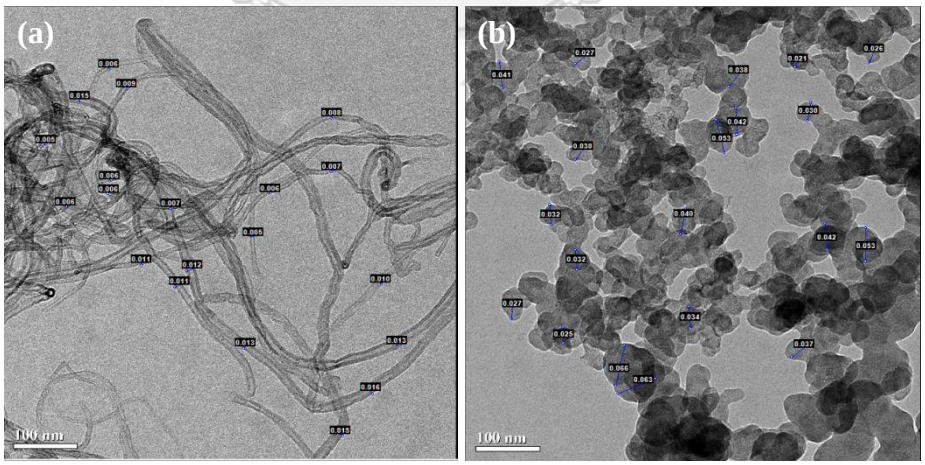

Fig. A2.1 Measured particle size of (a) CNT and (b) CB

Appendix B : CO_2 Absorption Flux Calculation

Three molar of monoethanolamine (MEA, 300 ml) was used as an absorbent in membrane performance test for 30 min. Captured carbon dioxide (CO_2) was measured by titration method which 2 ml of CO_2 absorbed MEA (3 M) was titrated with 1 M HCl and the gas was collected and measured in U-tube as shown in **Fig B.1**.

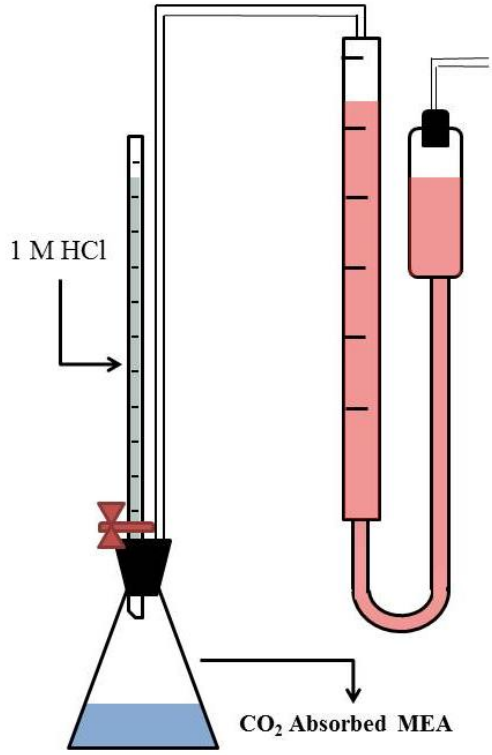

Fig. B.1 CO_2 loading analyzer

The CO_2 absorption flux was calculated as shown below;

$$V_{CO_2}(ml) = \frac{(V_{gas} - V_{HCl})}{2} \times 300 \quad \text{(B.1)}$$

$$n_{Absorbed\ CO_2}(mol) = \frac{(1\ atm) \times V_{CO_2}}{R(303\ K)}\ ; R = 82.057\ (ml \cdot atm/K \cdot mol) \quad \text{(B.3)}$$

$$J_{CO_2} = \frac{n_{Absorbed\ CO_2}}{t \times A_m} \quad \text{(B.4)}$$

which V_{CO_2} is CO_2 absorbed volume in 300 ml of 3 M MEA, V_{gas} is collected gas in U-tube (ml), V_{HCl} is added volume of HCl (ml), $n_{Absorbed\ CO_2}$ is mole of CO_2

absorption (mol), J_{CO_2} is CO_2 absorption flux (mol/m^{2}s), A_m is membrane contacted area (0.0024 m^2), and t is operation time (1800 s). The membrane was tested at ambient pressure and temperature (30 ˚C and 1 atm). The raw and calculation data were collected and shown in **Table B.1**.

Table B.1 Membrane testing conditions and calculations

Membranes	**Q_g (ml/min)**	**Q_l (ml/min)**	**V_{gas} (ml)**	**V_{HCl} (ml)**	**V_{CO2} (ml)**	**n_{CO2} (mol)**	**J_{CO2} (mol/m^2 s)**
26 wt% PVDF	320	158	14.4	12	360	0.0145	0.0034
	320	158	15.6	12	540	0.0217	0.0050
	320	153	16.5	12	675	0.0271	0.0063
0.5 wt% CNT/PVDF	320	155	14.4	12	360	0.0145	0.0034
	320	150	16.2	12	630	0.0253	0.0059
	320	152	16.2	12	630	0.0253	0.0059
1 wt% CNT/PVDF	320	164	14.4	12	360	0.0145	0.0034
	320	150	17.1	12	765	0.0308	0.0071
	320	150	16.8	12	720	0.0290	0.0067
5 wt% CNT/PVDF	320	160	15.6	12	540	0.0217	0.0050
	320	174	17.7	12	855	0.0344	0.0080
	320	152	18.0	12	900	0.0362	0.0084
10 wt% CNT/PVDF	320	158	24.6	12	1890	0.0760	0.0176
	320	152	22.2	12	1530	0.0615	0.0142
	320	164	21.6	12	1440	0.0579	0.0134
5 wt% CB/PVDF	320	160	16.2	12	630	0.0253	0.0059
	320	160	17.4	12	810	0.0326	0.0075
	320	160	16.8	12	720	0.0290	0.0067

Appendix C : List of Publication

P. Yaisanga, C. Klaysom, K. Maneeintr, and T.Charinpanitkul, Fabrication of carbon nanotube/polyacrylonitrile composite membrane for CO_2 capture, Proceeding of Pure and Applied Chemistry International Conference, 2016: p. 707-711.

VITA

Ms. Pacharaporn Yaisanga was born on May 7th, 1990. She obtained her Bachelor from Department of Chemical Engineering, Faculty of Engineering, Mahidol University in 2012 and continued studying her Master in Center of Excellence in Particle Technology (CEPT), Department of Chemical Engineering, Faculty of Engineering, Chulalongkorn University.